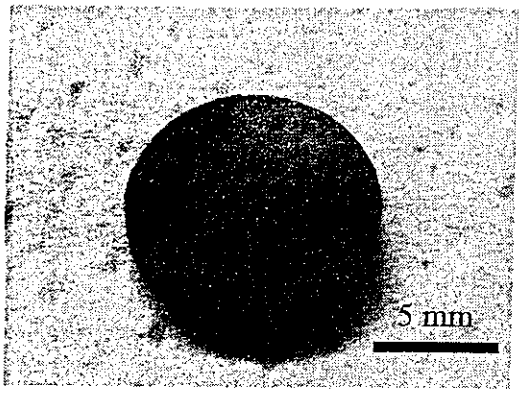

Figure 1. Photo of SWNT solid prepared by SPS method.

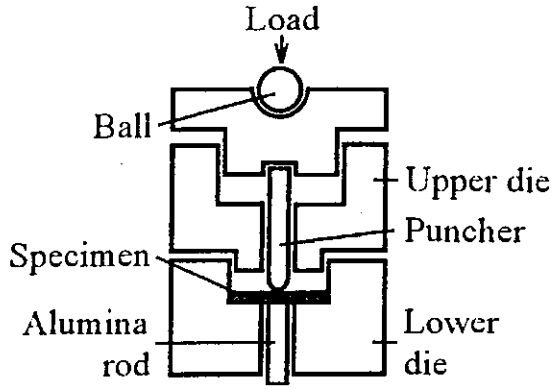

Figure 2. Schematic illustration of SP testing method.

3. SWNT 焼結体の機械的特性評価法

SWNT 焼結体の機械的特性評価には，SP 試験法による破壊特性評価を用い，破壊強度および破壊エネルギーの測定を行った．図 2 に SP 試験装置の概略図を示す．SP 試験法は周囲が単純支持された小型円盤状試験片の中央にパンチャーを介して荷重を加え，試験片裏面から Al_2O_3 ロッドを介して変位計を用いて荷重線変位を求め，得られた荷重ー荷重線変位より機械的特性および破壊挙動を評価する試験法である．試験時におけるパンチャーの移動速度は 0.05mm/min とした．応力 σ_{SP} および縦弾性係数 E_{sp} は有限要素法解析[5]に基づく式(1)，(3)により評価した．

$$\sigma_{SP}=\frac{P(1+\nu)}{t^2}\left[0.485\ln\frac{a}{t}+0.52+\frac{3}{2\pi(1+\nu)}\right]=\frac{S_0}{t^2}P \quad \cdots\cdots(1)$$

P ：パンチャー荷重

a ：支点間半径(下部ダイス半径)

t ：板厚

ν ：ポアソン比

一方，SP 試験片の無次元コンプライアンス $C(=E\delta/P)$ は次式で与えられる．

$$C=\frac{E\delta}{P}=f\left(\frac{t}{a}\right)\frac{3a^2(1-\nu)(3+\nu)}{4\pi^2}=f\left(\frac{t}{a}\right)C_0 \quad \cdots\cdots(2)$$

δ ：荷重線変位

$f(t/a)$ ：薄板理論に対する板厚の補正係数

ここで，$f(t/a)$ は有限要素法により求められている．

式(2)を用いて，縦弾性係数 E_{SP} を，コンプライアンス法に基づき，荷重ー荷重線変位曲線における初期の弾性域より次式を用いて求めた．

$$E_{SP}=f\left(\frac{t}{a}\right)\frac{3a^2P(1-\nu)(3+\nu)}{4\delta\pi t^3} \quad \cdots\cdots(3)$$

式(1)，(2)を組み合わせることにより，SP 試験片の応力 σ_{SP} は，

$$\sigma_{SP} \approx \frac{S_0}{t^2} P = E\left[\frac{S_0}{f(t/a)C_0 t}\delta\right] \cdots\cdots (4)$$

で表現できる．式(4)から横軸に応力σ_{SP}をとり，横軸に無次元化変位$[S_0/f(t/a)C_0 t]\delta$をとることにより，その初期勾配は材料の縦弾性係数Eを与えることになる．従って，上述の無次元化変位を用いることにより異なる板厚に対する荷重－変位曲線を比較できるものと考えられる．

4. 機械的特性の実験結果

図3に応力－無次元化変位曲線を示す．各試験片において負荷の初期段階においてはいずれも弾性変形を示しているが，精製を行っていないSWNTでは，荷重が最大値に達した後に急激に降下し，試験片が脆性破壊したことを示している．精製を行ったSWNT(1)では，最大荷重に達した後に一度荷重は低下するが，その後再び増加に転じ，徐々に荷重が低下する準脆性的な破壊挙動を示した．一方，精製を行ったSWNT(2)では，他の実験結果で見られた破壊挙動と大きく異なり，荷重の増加後にわずかな荷重低下を示すが，その後再び増加し最大荷重に達する破壊挙動を示し，変位の増加に伴い大幅な破壊エネルギーの向上が得られた．また，他の試験片に比べ破壊応力は約1.5倍の46.8MPaを得た．SP試験によって得られた各試験片の機械的特性を表2に示す．

5. SWNT焼結体に含まれる不純物の評価

走査型電子顕微鏡(SEM)，X線回折(XRD)およびラマン分光器を用いてSWNT焼結体に含まれる不純物の評価を行った．図4,5,6に各試験片破面のSEM画像とSWNT焼結体を粉砕した粉末のXRD測定結果を示す．精製を行っていないSWNTの破面(図4a)では，金属微粒子が凝集したと

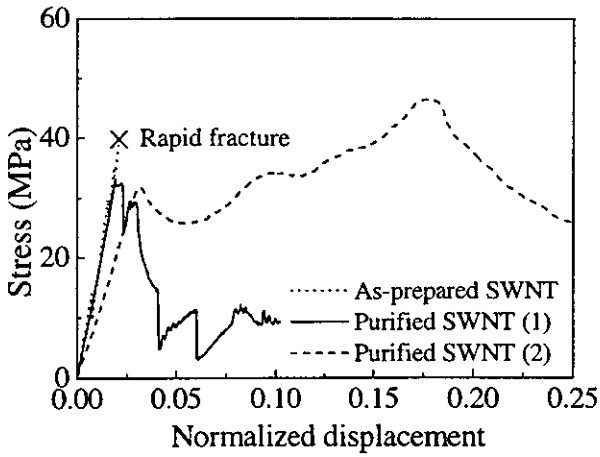

Figure 3. Relationship between stress and normalized displacement

Table 2. The mechanical properties of SWNT solids evaluated by SP testing method.

Sample type	Yong's modulus E_{sp} (GPa)	Fracture stress σ_{sp} (MPa)	Fracture energy G_{sp} (N/m^2)
As-prepared SWNT	0.74	33.6	0.40
Purified SWNT (1)	0.77	33.2	3.50
Purified SWNT (2)	0.63	46.8	35.52

思われる斑点状の模様が一面に観測され，XRD 測定(図 4b)においても，触媒金属に使用した Fe/Ni の存在が確認された．精製を行った SWNT (1)の破面(図 5a)では，斑点状の模様は局部的に観測されるものの，精製を行っていない SWNT に比べその量は少なかった．XRD 測定(図 5b)においても Fe/Ni ピークは測定されるものの，その強度は極めて低いものであった．一方，精製を行った SWNT (2)の破面(図 6a)，XRD 測定(図 6b)では，Fe/Ni の存在はほとんど認められなかった．

図 7 に各焼結体のラマン散乱スペクトルを示す．ラマン散乱測定は Ar レーザー光を使用した．スペクトルの 1590cm^{-1} 付近に見られるグラファイト由来の G-band と，アモルファスカーボンなどの不純物に由来する 1350cm^{-1} 付近に見られる D-band の強度比(G/D)を取ることにより，試料の純度を見積もることが可能である．精製を行った SWNT (2)の G/D 比は他のサンプルと比較し約 5~6 倍と高い強度比を示し，焼結体中にアモルファスカーボンなどの不純物をほぼ含まない焼結体であることが確認された．一方で，精製を行っていない SWNT および精製を行った SWNT (1)では，ブロードな D-band シグナルが認められ，その G/D 比は低く焼結体中にアモルファスカーボンなどの不純物の占める割合が高いことが確認された．

上述の SP 試験および不純物の評価に基づけば，SWNT 焼結体に含まれるグラファイトおよびアモルファスカーボンが破壊挙動に影響を及ぼしているものと考えられる．これらを多く含む精製を行っていない SWNT では，グラファイトおよびアモルファスカーボンが SWNT 焼結体の特性に支配的であるために，き裂が急速に破断まで至る脆性破壊が生じたと推察される．一方，精

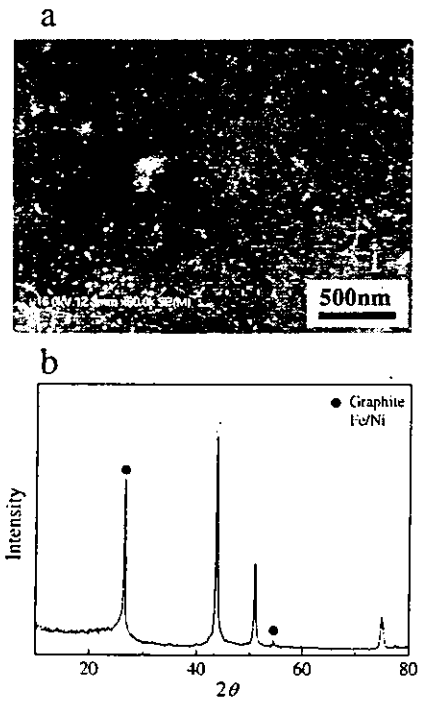

Figure 4 (Top) SEM photograph and (bottom) XRD profile of the As-prepared SWNT.

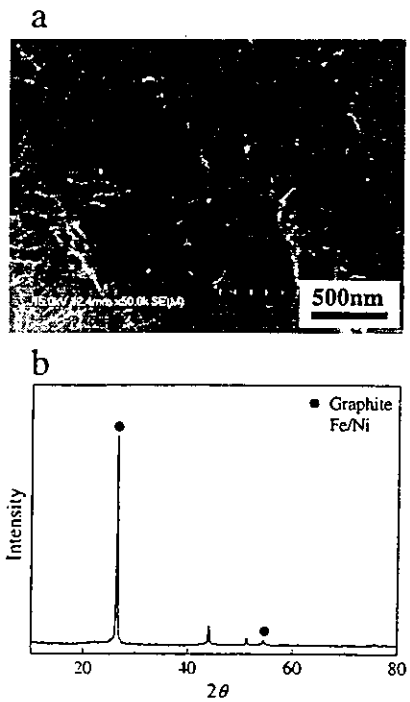

Figure 5 (Top) SEM photograph and (bottom) XRD profile of the Purified SWNT (1).

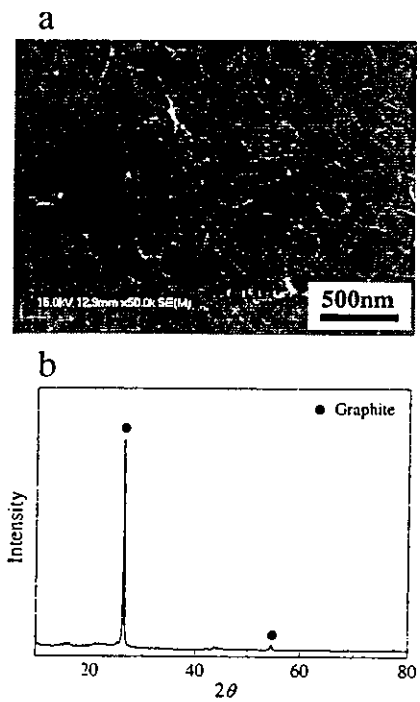

Figure 6 (Top) SEM photograph and (bottom) XRD profile of the Purified SWNT (2).

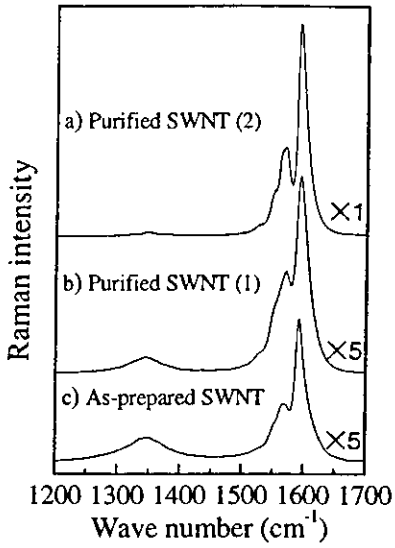

Figure 7. Raman spectra of a) Purified SWNT (2), b) Purified SWNT (1) and c) As-prepared SWNT after prepared by SPS method.

製を行ったSWNT (2)では，SWNTの存在比の高さから，SWNTの引き抜けに起因した準脆性的な破壊挙動を示したものと推察される．

6. 結言

本研究は単層カーボンナノチューブ焼結体に含まれる不純物が機械的特性に与える影響を評価することを目的とし，SPS法により作製したSWNT焼結体を対象としてSP試験法により破壊試験を行った．その結果，SWNT焼結体に含まれる不純物の量により，強度の向上および準脆性的な破壊挙動を示す試験片を得ることが可能であることが分かった．

最後に，本研究の一部は厚生労働省科学研究費補助金萌芽的研究先端医療技術推進事業(H14-ナノ-021)ならびに日本学術復興会特別研究事業の助成によるものである．

参考文献

1) Iijima, S., and Ichihashi, T., Single-shall carbon nanotubes of 1-nm diameter, *Nature*, 363, 603, (1993).

2) G-D. Zhan, J. D. Kuntz, J. Wan and A. K. Mukherjee, Single-wall carbon nanotubes as attractive toughening agents in alumina-based nanocomposites, *Nature Materials*, 2, 38, (2002).

3) Nishijima, H., Kamo, S., Akita. S. and Nakayama, Y., Carbon-nanotube tips for scanning probe microscopy: Preparation by a controlled process and observation of deoxyribonucleic acid, *Appl. Phys. Lett* 74, 26, 4061, (1999).

4) Mamoru, O., Sintering, consolidation, reaction and crystal growth by the spark plasma system (SPS). *Mater. Sci. Eng.* A287, 183, (2000).

5) Okuda, S., Saito, M., Hashida, T. and Takahashi, H., Small punch Testing Method for the Development of Functionally Gradient Materials, *Trans. JSME.* A57, 536, 248, (1991).

Appl. Phys. A 79, 85–87 (2004)
DOI: 10.1007/s00339-004-2599-9

Applied Physics A
Materials Science & Processing

Rapid communication

G.-H. JEONG[1,✉]
N. SATAKE[1]
T. KATO[1]
T. HIRATA[1]
R. HATAKEYAMA[1]
K. TOHJI[2]

Simple methods for site-controlled carbon nanotube growth using radio-frequency plasma-enhanced chemical vapor deposition

[1] Department of Electronic Engineering, Tohoku University, Sendai 980-8579, Japan
[2] Department of Geoscience and Technology, Tohoku University, Sendai 980-8579, Japan

Received: 14 July 2003/Accepted: 15 January 2004
Published online: 27 February 2004 •

ABSTRACT We demonstrate the validity of very simple methods for site-controlled carbon nanotube growth using a radio-frequency magnetron-type plasma-enhanced chemical vapor deposition technique. Enhanced plasma density and optimized ion-bombardment energy achieved by magnetic field introduction are found to be responsible for the uniform and well-aligned carbon nanotube growth. Based on these results, we attempted to perform experiments on site-controlled carbon nanotube growth using very convenient methods such as scratching or simply masking a substrate surface where carbonaceous materials deposit.

PACS 61.46.+w; 52.80.Pi; 81.15.Gh

1 Introduction

Because of their unique and prominent properties, carbon nanotubes have attracted a great deal of attention both scientifically and industrially. Especially, extensive studies have focused on the development of simple and controlled nanotube growth techniques for the purpose of industrial applications to various fields [1]. Concerning the site-selective growth, numerous techniques such as electron-beam lithography [2], a template method using porous materials [3], and ion-beam surface treatment [4] have been reported so far. When we use electron-beam lithography or the template method, which have been regarded as the representative techniques to prepare catalytic arrays, multi-walled carbon nanotubes (MWNTs) are generally produced in a highly site-controlled manner. However, their growth is limited to a very small area (in the case of the lithography technique) or involves following some cumbersome processes (in the case of the template method) such as wet etching and cleaning. On account of the relatively easy control of ion-bombardment energy and ion flux toward growing nanotubes, on the other hand, plasma-enhanced chemical vapor deposition (PECVD) has extensively been used for the individual and vertically aligned growth of the MWNTs in relation to their potential applications mainly as an electron emitter [5]. Here, we demonstrate very simple methods for the site-controlled MWNT growth in a quite large area using a radio-frequency PECVD (rf-PECVD) technique.

2 Experimental

In order to construct an rf (13.56 MHz) magnetron-type plasma apparatus, a magnetic field ($0 \leq B_z \leq 340$ G) is externally imposed parallel to a cylindrical rf electrode (3 cm in diameter) using solenoid coils [6]. Different from the prevailing parallel-plate PECVD units, the cylindrical rf electrode is made of Ni and surrounded by a grounded cylindrical chamber (13 cm in inner diameter and 30-cm long). This unique geometry gives rise to lower plasma sheath voltages at the rf electrode and higher plasma densities, which may endow optimal growth conditions. Essential plasma parameters such as plasma density n_e, electron temperature T_e, and plasma potential φ_p are measured by a Langmuir probe.

Figure 1a shows the effect of gas pressures on the radial profile of plasma density with $B_z = 170$ G. It is found that

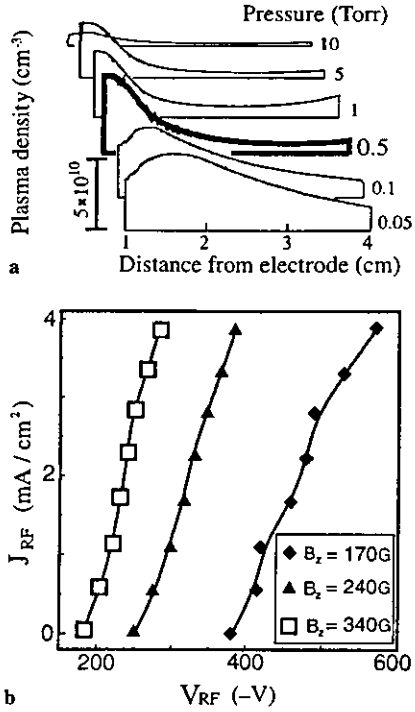

FIGURE 1 a Plasma density profiles in a radial direction for various gas pressures, b relationships between J_{rf} and V_{rf} for typical magnetic field strengths

✉ Fax: +81-22/263-9375, E-mail: hatak17@ec.ecei.tohoku.ac.jp

the plasma density is enhanced in the vicinity of the rf electrode and reaches a maximum when the working pressure is 0.5 Torr. It is to be noted that the product of electron-cyclotron frequency (ω_{ce}) by electron-neutral collision time (τ_{en}) is of the order of $\omega_{ce}\,\tau_{en} = 1$ under these conditions, which is an important quantity in magnetic confinement of plasmas. In addition to this, the dc voltage component (V_{rf}) of and the dc current density (J_{rf}) toward the rf electrode can be externally controlled as presented in Fig. 1b by connecting a dc power supply to it through a low-pass-filter circuit.

As a pretreatment [7], Ar sputtering has been performed for 15 min with the rf power of 1 kW. After this, a 15-min glow discharge (1-kW rf power, $CH_4 : H_2 = 9 : 1$) gives rise to vertically grown MWNTs on the powered rf-electrode surface. Field-emission scanning electron microscopy (FE-SEM, Hitachi S-4100) and field-emission transmission electron microscopy (FE-TEM, Hitachi HF-2000) are mainly employed to characterize the features of the carbon nanotubes grown.

3 Results and discussion

Firstly, according to Fig. 2a showing the feature of MWNTs grown for 3 min, it is observed that the MWNTs start to grow from, mainly, the top of protruding nano-islands (see inset) with various diameters. Thus, these islands formed by Ar plasma treatment are considered to play an important role in the nanotube formation, particularly at the primitive stage of the nanotube formation. Although carbon nanotube tip-growth mechanisms, which are commonly observed in the case of PECVD and explained in terms of surface adsorption on the catalyst, decomposition, diffusion, and final precipitation of carbon species in the form of a honeycomb structure, are frequently predicted in the literature [1, 8, 9], the specific investigation of the nucleation stage has almost never been reported. Very recently, we have reported the time evolution of the nucleation and further vertical growth using the PECVD method and found that the nanotube nucleation process firstly takes place through the catalyst tip formation preferentially from the protruding nano-islands due to an enhanced sputtering effect by the electric field concentration at the topmost region of the nano-islands, as shown in the inset of Fig. 2a [10].

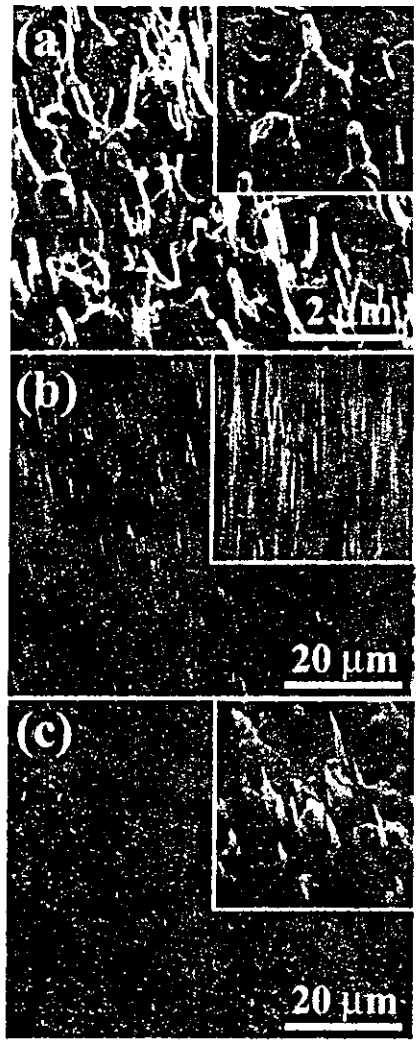

FIGURE 2 FE-SEM images. **a** After 3-min nanotube growth, **b** uniform and well-aligned MWNTs, **c** MWNT structure damaged by plasma ion bombardment

In order to investigate effects of magnetic field in our magnetron-type rf-PECVD, the dc component of the rf electrode, V_{rf}, is externally changed for typical magnetic fields (170 and 340 G) under the conditions of 0.5 Torr, $CH_4 : H_2 = 9 : 1$, and the rf power of 1000 W for 15 min. As we can see in Fig. 2b, uniform, dense, and well-aligned MWNTs grow in the externally biased case of $J_{rf} = 1.5\ \mathrm{mA/cm^2}$, $V_{rf} = -235$ V. On the other hand, when V_{rf} becomes extremely low, which is accompanied with an increase of ion flux ($J_{rf} = 4.0\ \mathrm{mA/cm^2}$, $V_{rf} = -570$ V), the nanotubes once formed are damaged due to a sputtering effect by both the high ion-bombardment energy and a surplus of ion flux from the plasma, as shown in Fig. 2c. From this result, it is clearly indicated that not merely ion flux, J_{rf}, but also ion-bombardment energy, V_{rf}, has to be optimized for the dense and well-aligned nanotube growth.

As explained above, the PECVD method is advantageous to controlled nanotube growth because the configuration and structure of resultant nanotubes grown can be varied by controlling the ion flux and the bombardment energy, which has not seen in any other nanotube formation methods. Utilizing this versatility of the PECVD method, we attempt to control the nanotube growth site in a simple way. Before inducing the mixture-gas discharge, the polished Ni surface was scratched linearly using a commercial sandpaper. After that, the mixture gas is discharged without the plasma pretreatment under the same condition of Fig. 2b. Figure 3 shows a FE-SEM image of MWNTs which are produced in the form of a linear array in this case. When the Ni surface is scratched, linearly arrayed projections are formed along both sides of the scratch line. Since these projections are considered to play the same role as the nano-islands in Fig. 2a, vertically well-aligned MWNTs are finally produced in a controlled manner.

On the other hand, we also attempt to produce the MWNTs in a large and selected area under the similar condition of Fig. 2c. In this situation, a region

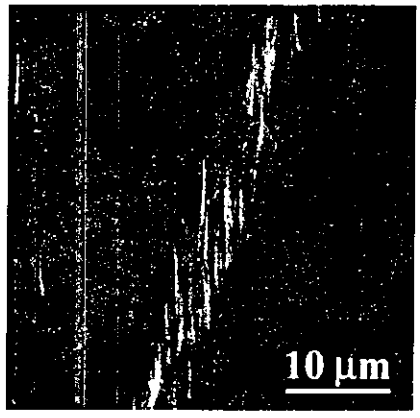

FIGURE 3 FE-SEM image showing the linearly arrayed MWNTs grown in the case of using the scratching method

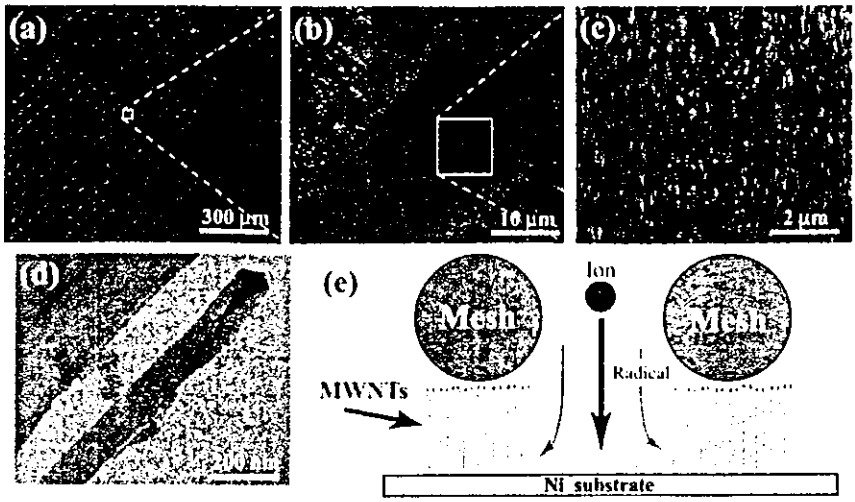

FIGURE 4 a, b, and c FE-SEM images showing the site-selectively grown MWNTs in a large area; the rectangular regions marked by *dotted lines* in (a) and (b) correspond to the images of (b) and (c), respectively, d FE-TEM image of an individual MWNT, e schematic illustration of the proposed model

of the rf-electrode surface, which is exposed to the plasma, is baneful to the vertical growth due to the intensive sputtering. Here, we introduce a commercial mesh in order to wrap a surface of a Ni substrate attached onto the rf electrode and therefore mask it to avoid the harmful sputtering phenomenon.

FE-SEM images in Fig. 4 show that the MWNTs are distributed with a high uniformity in a large area (see, in particular, Fig. 4a) and their location strongly supports the site-controllability (Fig. 4b and c). It is found that the MWNTs are formed beneath the mesh with a high density and a growth rate of 0.1 μm/min. On the contrary, it is hard to confirm the existence of MWNTs grown in the plasma-exposed regions, which is due to the direct sputtering of the high-energy positive ions, as already mentioned. A FE-TEM image of the individual MWNT in the same sample is given in Fig. 4d and reveals that the nanotube growth proceeds by the tip-growth mechanism because the Ni catalyst appears at the tube apex. Based on these results of the direct observations, a simple model describing the real situation is schematically illustrated as presented in Fig. 4e. In this study, it is conceived that MWNT growth characteristics beneath the mesh are similar to those of the thermal CVD rather than the usual PECVD because the Ni substrate surface is heated to ~ 650 °C by plasma ion bombardment and the affluent carbonaceous species such as CH_x radicals are supplied from the localized plasma state by the magnetic field introduction. It is an undeniable fact that these methods introduced here might not be superior to the electron-beam lithographic patterning or template technique in a sense of the precise site control. However, in the case of carrying out coarse patterning in a large area, our methods have the obvious advantage that we only need the really simple process, scratching or masking a plate. In addition, although our cylindrical PECVD system can not be directly applied to prevailing flat substrates, it is very helpful to apply it to a light source with a cylindrical geometry [11]. Moreover, if further detailed investigations are performed regarding the electric field concentration effect in the nanoscale, the selectivity in our methods is expected to be improved.

4 Conclusions

In summary, we have investigated the optimal plasma condition for the well-aligned MWNT growth and attempted to produce MWNTs in an easy manner with site-controlled growth using a cylindrical rf magnetron-type PECVD unit. It is found that the ion flux and the ion-bombardment energy have to be optimized in order to grow uniform, well-aligned, and density-controlled nanotubes. In a series of experiments it is finally demonstrated that very simple methods basically making use of the ion-bombardment energy are effective and available in a wide sense for the site-controlled carbon nanotube growth

ACKNOWLEDGEMENTS The authors thank K. Motomiya for his technical support. Part of this work was carried out under the Cooperative Research Project Program of the Research Institute of Electrical Communication, Tohoku University. This work was also supported by a Grant-in-Aid for Scientific Research from the Ministry of Education, Culture, Sports, Science and Technology, Japan.

REFERENCES

1 M. Meyyappan, L. Delzeit, A. Cassell, D. Hash: Plasma Sources Sci. Technol. **12**, 205 (2003)
2 V.I. Merkulov, D.H. Lowndes, Y.Y. Wei, G. Eres, E. Voelkl: Appl. Phys. Lett. **76**, 3555 (2001)
3 S. Fan, M.G. Chapline, N.R. Franklin, T.W. Tombler, A.M. Cassell, H. Dai: Science **283**, 512 (1999)
4 A. Gohel, K.C. Chin, K.Y. Lim, S.T. Tay, R. Liu, G.S. Chen, A.T.S. Wee: Chem. Phys. Lett. **371**, 131 (2003)
5 G. Pirio, P. Legagneux, D. Pribat, K.B.K. Teo, M. Chhowalla, G.A.J. Amaratunga, W.I. Milne: Nanotechnology **13**, 1 (2002)
6 N. Satake, G.-H. Jeong, T. Hirata, R. Hatakeyama, H. Ishida, K. Tohji, K. Motomiya: Physica B **323**, 290 (2002)
7 Z.F. Ren, Z.P. Huang, J.W. Xu, J.H. Wang, P. Bush, M.P. Siegal, P.N. Provencoi: Science **282**, 1105 (1998)
8 T. Hirao, K. Ito, H. Furuta, Y.K. Yap, T. Ikino, S. Honda, Y. Mori, T. Sasaki, K. Oura: Jpn. J. Appl. Phys. **40**, L631 (2001)
9 Y.S. Woo, I.T. Han, Y.J. Park, H.J. Kim, J.E. Jung, N.S. Lee, D.Y. Jeong, J.M. Kim: Jpn. J. Appl. Phys. **42**, 1410 (2003)
10 T. Hirata, N. Satake, G.-H. Jeong, T. Kato, R. Hatakeyama, K. Motomiya, K. Tohji: Appl. Phys. Lett. **83**, 1119 (2003)
11 J.M. Bonard, T. Stöckli, O. Noury, A. Châtelain: Appl. Phys. Lett. **78**, 2775 (2001)

Large-Scale Production of Ba^{2+}–Alginate-Coated Vesicles of Carbon Nanofibers for DNA-Interactive Pollutant Elimination

Bunshi Fugetsu,* Shuya Satoh, Toshikazu Shiba,[1,2,3] Taeko Mizutani,[2] Yoshinobu Nodasaka,[4] Keiji Yamazaki,[5] Kiyoko Shimizu,[6] Masanobu Shindoh,[4] Ken-ichiro Shibata,[4] Norio Nishi, Yoshinori Sato,[7] Kazuyuki Tohji,[7] and Fumio Watari[4]

Graduate School of Environmental Earth Science, Hokkaido University, Sapporo 060-0810

[1]Regenetiss Co., Ltd., 1-5-17, Okaya, Akabane, Nagano 394-0002

[2]Millennium project, Frontier Research Division, Fujirebio Inc., 51, Komiya, Hachioji, Tokyo 192-0031

[3]Department of Oral and Maxillofacial Surgery, Matsumoto Dental University School of Dentistry, Shiojiri 399-0781

[4]Graduate School of Dental Medicine, Hokkaido University, Sapporo 060-8586

[5]Otsuka Electronic Co., Ltd., 1-6 Azuma-cho, Hachioji, Tokyo 192-0082

[6]Hokudo Co., Ltd., Bioscience Division, Abuta-cho, Abuta-gun, Hokkaido 049-5613

[7]Graduate School of Environmental Studies, Tohoku University, Sendai 980-8579

Received March 24, 2004; E-mail: hu@ees.hokudai.ac.jp

Ba^{2+}–alginate coated vesicles (Ba^{2+}–ALG) containing highly dispersed carbon nanofibers (CNFs) were successfully produced for the first time using an encapsulation technique. These Ba^{2+}–ALG/CNFs composite vesicles showed high capabilities in trapping DNA-interactive types of chemicals. For example, 10.0 mL of the vesicles took 0.43 μmol of ethidium ions up from contaminated water within 8 min. Biocompatibility experiments performed in vitro and in vivo provided promising results, suggesting potential applications in in-situ environmental remediation. Kilogram quantities of the Ba^{2+}–ALG/CNFs composite vesicles can be produced within a few hours.

DNA-interactive chemicals, such as ethidium ions, are capable of interacting with DNA with high affinities. This type of chemical is responsible for causing DNA damage and/or frame-shift mutagenesis induction, also known as the key-initial processes in carcinogenesis.[1–3] We demonstrated in our previous studies[4–7] that materials having DNA as functional sites, such as Ba^{2+}–alginate coated vesicles containing double-stranded DNA (purified from salmon milt), are capable of trapping this type of chemical from contaminated waters. DNA leakage, which results in performance degradation and a limited lifetime of the functional materials, however, has been a major drawback of these materials.[8]

In this study, we use carbon nanofibers (CNFs) as the functional sites for trapping DNA-interactive chemicals. Adsorbents with high capabilities were obtained successfully by encapsulating the highly dispersed CNFs in Ba^{2+}–alginate coated vesicles. In recent years, carbon nanomaterials, especially the so-called carbon nanotubes (CNTs), discovered first by Iijima,[9,10] have attracted great attention due to their unusual morphologies. An analytical chemical study carried out by Cai and co-workers[11] demonstrated that multi-walled CNTs (MWCNTs) can trap some aromatic chemicals, such as bisphenol A, 4-*n*-nonylphone, and 4-*tert*-octylphenol from contaminated water by passing the contaminated water through a cartridge filled with MWCNTs. The targeted species trapping was achieved by the hexagonally arrayed carbon atoms of the graphite sheets of the external faces of the MWCNTs.[11,12]

CNFs are built up also by hexagonally arrayed carbon atoms with the 002 planes being piled up along the direction of the fiber axis. These graphite platelets stacked in a perfectly arranged conformation resulted in generating a unique system comprising entirely of slit-shaped wall-nanopores.[13] If these wall-nanopores can be also activized for trapping DNA-interactive chemicals, higher elimination efficiencies than can be achieved with MWCNTs can be obtained.

Experimental

Dispersing CNFs Using Alginate. Sodium alginate (viscosity and pH at 20 °C were 300–400 cP and 6.0–8.0, respectively, for a 20.0-mg/mL aqueous solution), the dispersing agent used throughout this study, was obtained from Wako Chemical Industries (Osaka, Japan). Sodium alginate (Na^+–ALG) was dissolved in deionized water to prepare the aqueous Na^+–ALG solutions. CNFs (diameter, 50–250 nm; length, 2–15 μm; purity > 90%; those produced in the laboratory were based on the chemical vapour deposition;[14] Figs. 1A and B show the SEM and TEM images) were added to the aqueous Na^+–ALG solutions and were well-mixed by a combination of high-shear mixing and sufficient ultra-sonication. The aqueous Na^+–ALG/CNFs colloidal solutions were centrifuged at 4000 rpm for 30 min. A very small amount of black precipitate from the aqueous solution was observed (which was removed from the aqueous colloidal solution).

Published on the web October 9, 2004; DOI 10.1246/bcsj.77.1945

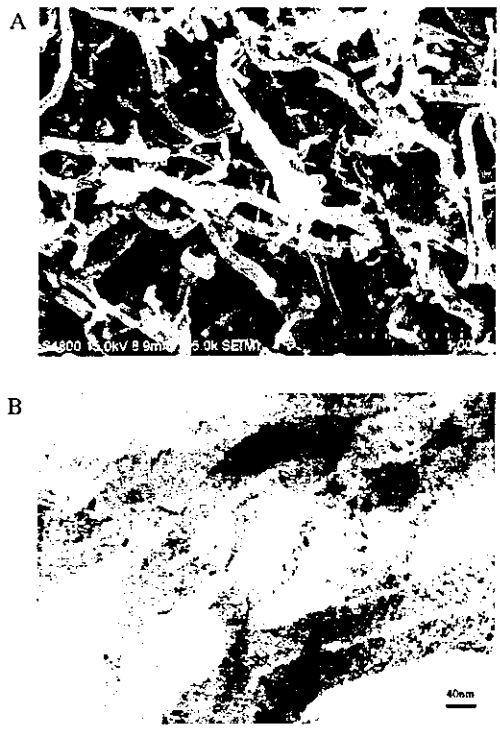

Fig. 1. SEM image (Fig. 1A) and TEM image (Fig. 1B) of the synthesized/purified carbon nanofibers (CNFs). SEM (Hitachi S4800) was operated at 15 kV; while TEM (Hitachi H-800) was operated at 200 kV. Platelet CNFs in which the 002 planes are piled up along the fiber axis direction together with the herringbone CNFs in which the 002 planes are distrusted on the two sides at an angle with respect towards the fiber axis were observed.

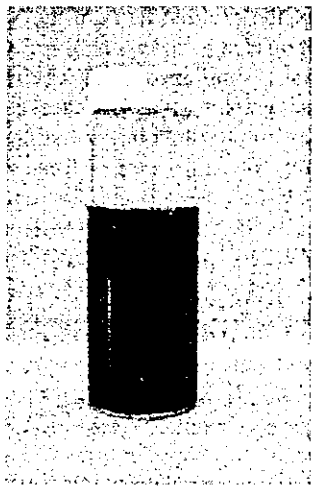

Fig. 2. A photograph of a 100-mL glass-vial containing CNFs being highly dispersed in the Na^+–ALG aqueous solution. Concentrations of CNFs and Na^+–ALG were 0.5 mg/mL and 20.0 mg/mL, respectively.

Figure 2 shows a photograph of a 100-mL glass vial containing the aqueous Na^+–ALG/CNFs colloids. Concentrations for CNFs and Na^+–ALG were 0.50 mg/mL and 20.0 mg/mL, respectively. No precipitation was observed from this aqueous colloidal solution during a three-week observation period. Aqueous Na^+–ALG/CNFs colloids with a high uniformity were obtainable up to a concentration of 1.0 mg/mL for CNFs using the 20.0 mg/mL aqueous Na^+–ALG solution as the dispersing solution. The uniformity of the aqueous Na^+–ALG/CNFs colloids was measured by calculating the linearity of the calibration curve for CNFs in the Na^+–ALG/CNFs colloidal solutions using UV–vis at 260 nm as the detection. Zeta potentials of the aqueous Na^+–ALG/CNFs colloids were measured using an electrophoretic light scattering spectrophotometer (ELS-8000, Otsuka Electronics, Osaka, Japan). FT-IR spectra of Na^+–ALG in the aqueous Na^+–ALG/CNFs colloids were measured using a FT/IR-460 (Jasco, Tokyo, Japan).

Biocompatibility Tests. Normal human fibroblasts (HF) were used as the typical cells (obtained from BioWhitteker Inc.) to perform the in vitro experiments. A MTS [3-(4,5-dimethylthiazol-2-yl)-5-(3-carboxymethoxyphenyl)-2-(4-sulfophenyl)-2*H*-teraazolium] cell proliferation assay kit was purchased from Promega. Dulbecco's modified Eagle's minimal essential medium (D-MEM), L-glutamine, and fetal bovine serum (FBS) were purchased from Sigma. The aqueous Na^+–ALG/CNFs colloidal solution containing 1.0 mg/mL of CNFs and 20.0 mg/mL of Na^+–ALG was diluted to 1/10, 1/100, and 1/1000 with D-MEM containing 5.0% FBS and 50 μg/mL kanamycin. An aqueous solution containing Na^+–ALG alone (20.0 mg/mL; the control vehicle) was also diluted to the same degree with the same medium as for Na^+–ALG/CNFs. HF were seeded in 96-multiwell plates at 2×10^3 cell/well and maintained in 200 μL D-MEM containing 10% FBS and 50 μg/mL kanamycin for 3 days at 37 °C. The medium was replaced with the medium containing the Na^+–ALG/CNFs or the control vehicle and were further incubated for 1–7 days at 37 °C. After the incubation, cell growths were evaluated by MTS assay. For the MTS assay, the medium was substituted for 100 μL of Eagle's minimal essential medium (without Phenol Red) containing 333 μg/mL MTS and 25 μM phenazine methosulfate solution. After incubation for 2 h at 37 °C, the absorbance at 485 nm of each well was measured. The cell growth was calculated from the value of A_{485} at 2 h after MTS processing.

Eight 8-week-old Jcl:SD male rats (purchased from Clea Japan, Inc.) were used to perform the in vivo experiments. These rats were quarantined and acclimatized for six days. One was used without any administration while the others were single dosed orally using a stomach tube. The dose values were 10 mg/kg for CNFs and 200 mg/kg for Na^+–ALG of the body weight. Gross observations and body weights were recorded weekly. During the term of observation, animals were starved for 16 h, anesthetized, and then blood and serum samples were collected. Necropsy was also performed for observing changes in the glandular stomach.

Encapsulating CNFs. An IER-20® system (Inotech, Dottikon, Switzerland) was used for encapsulating CNFs to form Ba^{2+}–alginate coated vesicles. The IER-20® system consisted of a syringe and a pump, a pulsation chamber, a vibration system, a nozzle, an electrode, an ultra-sonication vibration system along with an electrostatic supply system, and an O-ring-shaped electrode. The aqueous Na^+–ALG/CNFs colloids were forced into the pulsation chamber using the syringe pump. These aqueous colloids were then passed through the precisely drilled sapphire-nozzle (nozzle size, 300 μm) and were separated into droplets of equal size on exiting the nozzle. These droplets passed through the electrostatic field between the nozzle and the ring electrode and acquired electrostatic charges on their surfaces. Electrostatic repulsion forces dispersed the droplets as they fell in to the hardening solution, i.e., the aqueous solution containing 100 mM of barium chloride. The resultant vesicles were rinsed thoroughly

with deionized water using a 100 μm mesh sieve. Reference vesicles (without containing CNFs) were also prepared under these identical experimental conditions.

Adsorptive Capability Studies. Three 45-mL conical-bottomed tubes, each containing 10.0 mL of the reference vesicles, the vesicles containing highly dispersed CNFs, and the vesicles containing low-dispersed CNFs, were held vertically using a tube-stand, 15.0 mL of a 30.0 μM ethidium bromide aqueous solution were then added to each of the tubes. At about ten minutes after mixing the ethidium solution with the vesicles, approximately 3 mL of the bulk-phase solutions were collected and measured using a UV–vis spectrometer (Jasco UV-550).

Results and Discussion

Insights in to the Dispersion Mechanism. A characteristic absorption band derived from the CNFs is seen at around 260 nm for the aqueous Na^+–ALG/CNFs colloidal solutions. The linearity, r^2, of the calibration curve for CNFs in the aqueous Na^+–ALG/CNFs colloidal solutions at 260 nm was found to be better than 0.9986, indicating a high uniformity of the aqueous Na^+–ALG/CNFs colloidal solutions. Samples used for deriving the calibration curve were the aqueous Na^+–ALG solutions containing 0, 0.1, 0.2, 0.3, 0.4, and 0.5 mg/mL of the CNFs with the concentration of Na^+–ALG in each sample being fixed at 20.0 mg/mL. The stability of the aqueous Na^+–ALG/CNFs colloids was measured by calculating the concentration of the CNFs versus the sediment time, similar to the method reported by Jiang and co-workers.[15] Changes in the CNF concentrations were found to be smaller than 0.4% over three-weeks at room temperature.

The zeta potentials of the Na^+–ALG/CNFs colloids were measured. Zeta potential values, ζ, were calculated from the particle velocities based on the Helmholtz–Smoluchowski equation ($\zeta = 4\pi\mu\eta/D$, where, μ, η, and D are the electrophoretic mobility, viscosity, and the dielectric constant of the liquid in the boundary layer, respectively).[16] As can be seen from the ζ vs pH plots (Fig. 3), the maximum ζ value of the Na^+–ALG/CNFs colloids was −58.03 mV. This again indicates a high stability (repulsion) of the Na^+–ALG/CNFs colloids. The ζ vs pH plots (Fig. 3) for the Na^+–ALG/CNFs colloids and that for the aqueous solution containing Na^+–ALG alone were virtually identical, indicating the zeta potentials of the Na^+–ALG/CNFs colloids are governed by alginate ions. A decrease in the absolute value of ζ is seen for both samples as the pH decreased (pH of the samples were adjusted using 1.0 mol L^{-1} HCl) for all pH value studies. This implies that alginate attached tightly to the CNFs throughout the entire pH range. Note the Na^+–ALG/CNFs colloids condensed as the pH reached smaller values (2.99 and 1.51).

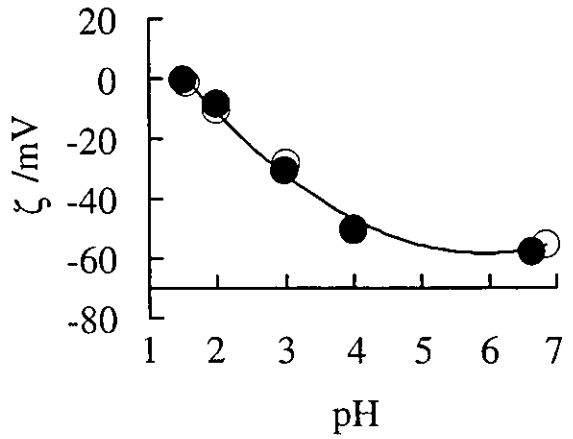

Fig. 3. Zeta potential (ζ) of the aqueous Na^+–ALG/CNFs colloids (●, 0.50 mg/mL for CNFs and 20.0 mg/mL for Na^+–ALG) and ζ of the aqueous solution containing Na^+–ALG alone (○, 20.0 mg/mL of Na^+–ALG) versus pH.

Alginate is a linear, water-soluble 1,4-linked copolymer of β-D-mannuronate (M) and/or α-L-guluronate (G). M and G can be arranged in homopolymeric [poly(β-D-mannosyluronate, M–M–M)] and poly(α-L-gulosyluronate, G–G–G) or heteropolymeric (M–G–M) blocks,[17,18] as illustrated in Fig. 4. FT-IR spectra of alginate alone (the reference sample) and the Na^+–ALG/CNFs colloids were measured, as shown in Fig. 5. The typical characteristic bands found for the reference

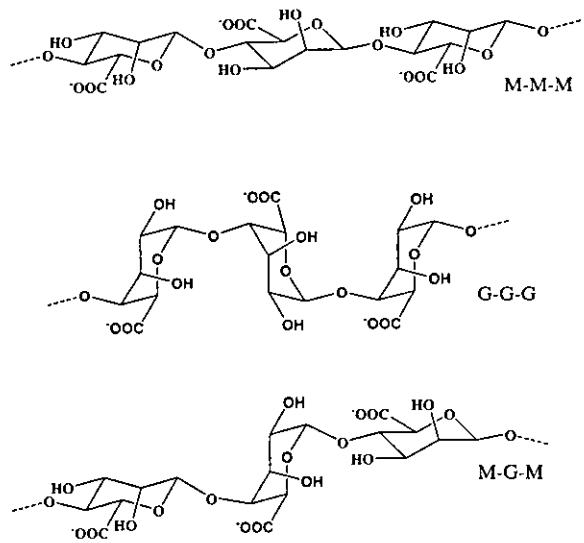

Fig. 4. Three possible molecular structures of alginate. The homopolymeric M–M–M- and G–G–G- and M–G–M-linked alginate.

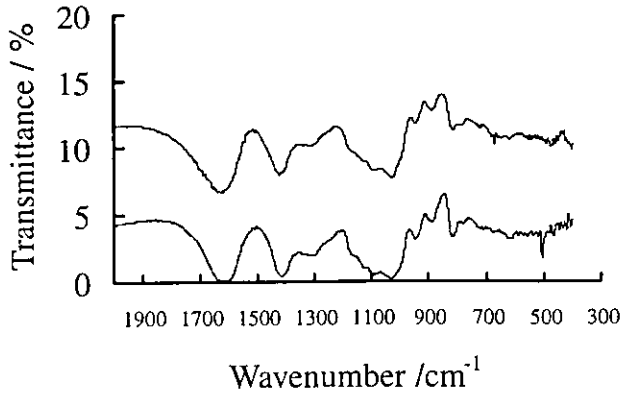

Fig. 5. FT-IR spectra of Na^+–ALG (upper-trace) and that of Na^+–ALG/CNFs colloids (lower-trace) in the solid state using the potassium bromide (KBr) pellet method.

sample (without containing CNFs) were (i) 1627.63 and 1419.35 cm^{-1} (carboxylate), (ii) 947.84 cm^{-1} (α 1 → 4 linkage), and (iii) 890.95 cm^{-1} (α-L-gulopyranuronic ring), respectively. While for Na^+–ALG/CNFs, they were (i) 1613.16 and 1413.57 cm^{-1}, (ii) 943.98 cm^{-1}, and (iii) 887.8 cm^{-1}, respectively. These shifts (decrease) in the alginate characteristic bands again indicate alginate being attached tightly to the CNFs. The characteristic band of the sugar backbones increased from 811.88 cm^{-1} in the reference sample (alginate alone) to 814.77 cm^{-1} in the Na^+–ALG/CNFs, suggesting the attaching of alginate to the CNFs is governed by their sugar backbones.

From these experimental observations, we suggest that complexes, i.e., alginate/CNFs, were formed in the aqueous Na^+–ALG/CNFs colloidal solutions. This can be attributed to the hydrophobic interactions occurring between the sugar backbones of alginate and the external surfaces of CNFs. The negatively charged moieties of the alginate/CNFs complex, i.e., the carboxylate groups, produce high zeta potentials, which stabilize the complexes in the aqueous electrolyte solutions.

Biocompatibility of Alginate/CNFs. Adsorbents of high biocompatibility are highly desirable in environmental remediation, especially in the case of in situ elimination of the targeted pollutants from the contaminated animals. In the in vitro experimental study with normal human fibroblasts (HF) as the typical cells, the relative cell growth (RCG), which was calculated by dividing a mean value of the treated cells by a mean value of untreated cells (cultured with 5% FBS), was found as high as 100 ± 5% at 1-day and 2-days after the administration of Na^+–ALG/CNFs and/or Na^+–ALG. RCG were better than 85 ± 5% even at 7-days after the administration. On the other hand, in the in vivo experimental study with rats as the typical animals, an increase in white blood cells (WBC) was observed at 1-week and 2-weeks after the administrations (WBC, μL^{-1}, increased from 5100 in the untreated rat to 7700 and 8100 in the rats given the control, while they increased to 7900 and 8400 for the rats given the Na^+–ALG/CNFs colloids). The β-globulin fraction also increased from 16.2% in the untreated rat to 21.7% and 21.5% in the rats treated with Na^+–ALG and/or Na^+–ALG/CNFs. Deep plica of the glandular stomach were observed at 1-week after the administration with Na^+–ALG and/or Na^+–ALG/CNFs. Changes in the other parameters were smaller than ±10%. All hematological and biochemical data recovered to normal levels 3-weeks after the administration. Both in vitro- and in vivo-experiments showed that alginate and the alginate/CNFs complexes had no or very little detrimental impact on the cells/animals studied in this study.

Adsorptive Capability of the Vesicles. Three gelling solutions, (i) an aqueous solution containing sodium alginate alone at 20.0 mg/mL, (ii) CNFs at 0.5 mg/mL highly-dispersed in 20.0 mg/mL Na^+–ALG solution, and (iii) CNFs at 0.5 mg/mL simply dispersed (mixed by ultra-sonication for 5 min) in 20.0 mg/mL Na^+–ALG solution, were prepared and used for preparing the reference vesicles (those did not contain CNFs), the vesicles containing highly dispersed CNFs, and the vesicles containing low-dispersed CNFs, respectively. A typical microscopic observation of the vesicles containing highly dispersed CNFs are shown in Fig. 6. Vesicles having a diameter in the range of 400–800 micrometers were observed. The nozzle diameter strongly influenced the vesicle size. Generally, vesicles are produced with an average diameter two times larger than the nozzle diameter. However, the average vesicle diameter can be adjusted by about ±20% by varying the jet velocity and the vibration frequency. Kilogram quantities of the vesicles can be produced within a few hours using this encapsulation system. The Ba^{2+}–ALG/CNFs composite vesicles are both chemically and mechanically stable, and are much heavier than water (hence it is easy to isolate the vesicles from water).

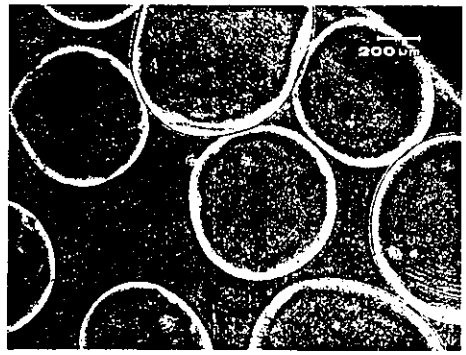

Fig. 6. Microscopic observation of the Ba^{2+}-alginate coated vesicles containing highly dispersed CNFs. The vesicles were produced using an aqueous colloidal solution containing 0.50 mg/mL CNFs and 20.0 mg/mL Na^+–ALG as the gelling solution with an aqueous solution containing 100 mM $BaCl_2$ as the gelatinizing solution.

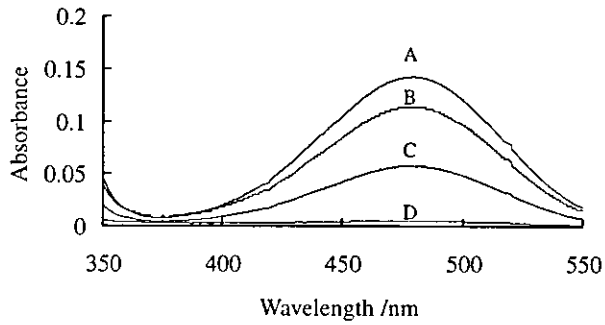

Fig. 7. UV–vis absorptions of an aqueous solution containing 30.0 μM ethidium bromide (A-trace); 15 mL of this 30 μM ethidium bromide solution being mixed with, the Ba^{2+}–alginate vesicles (reference vesicles; B-trace), the vesicles containing low-dispersed CNFs (C-trace), and the vesicles containing highly dispersed CNFs (D-trace) at 10 min after the solution/vesicles mixing.

Ethidium ions were chosen as the typical DNA-interactive species. They are highly water-soluble and used worldwide as an intercalating fluorescent dye for detecting DNA. Fifteen millilitres of the model contaminated water (prepared by dissolving ethidium bromide in deionized water at a concentration of 30.0 μM) was mixed with 10.0 mL of the vesicles. At about ten minutes after the mixing, approximately 3 mL of the bulk-phase solutions were collected and were measured using a UV–vis spectrometer. Figure 7 shows the results. The absorbance of the model contaminated water before the treatment, i.e., the 30.0 μM ethidium bromide aqueous solution, at

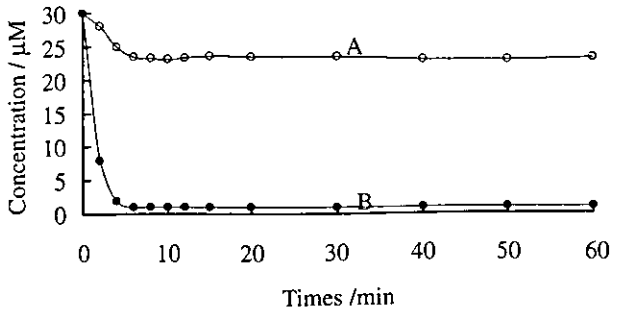

Fig. 8. Changes in concentrations of ethidium ions as a function of the contact time for a 15.0 mL of an aqueous solution containing 30.0 μM ethidium bromide after mixing that solution with 10.0 mL of the reference (Ba^{2+}–ALG) vesicles (upper-trace) and with the Ba^{2+}–ALG/CNFs composite vesicles (lower-trace).

480 nm was as high as 0.142. This, however, dropped to 4.9×10^{-3} after mixing this solution with the vesicles containing highly dispersed CNFs. Mixing the contaminated water with the vesicles containing low-dispersed CNFs also resulted in lowering the absorbance (which dropped to 0.058). This change, however, was much smaller than that observed for the vesicles containing highly dispersed CNFs. The control vesicles showed very little capability in trapping ethidium ions, suggesting the uptake of the targeted species is governed by the CNFs.

Figure 8 shows changes in the concentration of ethidium ions in the aqueous solution as a function of the contact time (15.0 mL of the 30.0 μM ethidium bromide aqueous solution were mixed with 10.0 mL of the vesicles containing the highly dispersed CNFs). The concentration of ethidium ions in the aqueous solution decreased rapidly as the contact time increased. It reached 0.98 μM and remained unchanged at about 8 min after mixing the solution with the Ba^{2+}–ALG/CNFs composite vesicles. In other words, 10.0 mL of the Ba^{2+}–ALG/CNFs composite vesicles took 0.44 μmol of the ethidium ions up and this uptake was accomplished within 8 min. The adsorptive experiments were performed three times, and the average value of the capacity for trapping ethidium ions for 10.0 mL of the vesicles obtained using the aqueous Na^{+}–ALG/CNFs colloidal solution containing 0.5 mg/mL for CNFs and 20.0 mg/mL for Na^{+}–ALG as the gelling solution was as high as 0.43 μmol (RDS < ±1.2%).

Identical experiments were also performed using Ba^{2+}–alginate coated vesicles containing highly dispersed multi-walled carbon nanotubes (MWCNTs) as the adsorbents. MWCNTs (diameter, 20–40 nm; length, 1–5 μm, purity > 90%, as recommended by the manufacturer) were purchased from Nano Lab. and were used as received. Methods for preparing the aqueous Na^{+}–ALG/MWCNTs colloids, Ba^{2+}–ALG/MWCNTs composite vesicles, and for studying the capability for trapping ethidium ions were the same as for the CNFs. The capacity for trapping ethidium ions was found to be 0.42 μmol (RDS < ±1.3%, $n = 3$) for 10.0 mL of the Ba^{2+}–ALG/MWCNTs vesicles obtained using an aqueous solution containing 0.50 mg/mL MWCNTs and 20.0 mg/mL Na^{+}–ALG as the gelling solution. This capacity value is virtually identical to that of the Ba^{2+}–ALG/CNFs composite vesicles, indicating the ethidium ions were unable to distribute in to the wall-nanopores of the CNFs. In other words, to accumulate the DNA-interactive chemicals in the wall-nanopores, it is necessary to expand the inter-planar distance among the graphite platelets of the CNFs.

Conclusion

Dispersing carbon nanofibers and/or nanotubes with a high uniformity into aqueous solutions is crucial for achieving the goal of utilizing these fascinating materials as high-performance adsorbents for absorbing/eliminating DNA-interactive type chemicals. The major goal in this study was achieved using alginate as the dispersing agent. Alginate is a non-toxic, naturally occurring linear polysaccharide (found widely in brown seaweed). Its gelling properties, together with its high biocompatibility, can generate a number of analytical-chemical, environmental, and biotechnological applications. Our dispersing approach based on alginate provides advantages over the previous methods:[19-25] (i) aqueous colloidal solutions containing CNFs and/or CNTs in pristine forms can be prepared in large-scales in a single step with a very simple manipulation procedure, (ii) the resultant aqueous colloids are highly biocompatible, and (iii) the colloids can be rearranged further as vesicles, providing a desirable approach to utilizing these nano-sized materials for macro-scaled applications. The selectivity of the Ba^{2+}–ALG/CNFs (also the Ba^{2+}–ALG/CNTs) composite vesicles for adsorbing DNA-interactive chemicals, especially for aromatic compounds having planar structures, is high. This is because the hexagonal arrays of the carbon atoms of the graphite sheets are the functional sites for trapping the targets. Note that columns packed with the entire CNFs and/or MWCNTs may also provide high trapping capabilities. They are, however, impractical for large-scale water treatment. This is because of the high backpressure that must be overcome to drive water through the packed column.

This study was partly supported by Grant-in-Aid for Research on Nano-medicine #H14-nano-021 from the Ministry of Health, Labor and Welfare.

References

1 E. C. Miller and J. A. Miller, *Cancer*, **47**, 2327 (1981).
2 B. N. Ames, *Science*, **204**, 587 (1979).
3 W. P. Watson, C. Bleasdale, and B. T. Golding, *Chem. Br.*, **1994**, 661.
4 K. Iwata, T. Sawadaishi, S. Ninishimura, S. Tokura, and N. Nishi, *Int. J. Biol. Macromol.*, **18**, 149 (1996).
5 M. Yamada, K. Kato, K. Shindo, M. Nomizu, M. Haruki, N. Sakairi, K. Ohkawa, H. Yamamoto, and N. Nishi, *Biomaterials*, **22**, 3121 (2001).
6 M. Yamada, K. Kato, M. Nomizu, N. Sakairi, K. Ohkawa, H. Yamamoto, and N. Nishi, *Chem.—Eur. J.*, **8**, 1407 (2002).
7 M. Yamada, K. Kato, M. Nomizu, K. Ohkawa, H. Yamada, H. Yamamoto, and N. Nishi, *Environ. Sci. Technol.*, **36**, 949 (2002).
8 D. Umeno, T. Kano, and M. Maeda, *Anal. Chim. Acta*, **365**, 101 (1998).
9 S. Iijima, *Nature (London)*, **354**, 56 (1991).

10 S. Iijima and T. Ichihashi, *Nature (London)*, **363**, 603 (1993).
11 Y. Cai, G. Jiang, J. Liu, and Q. Zhou, *Anal. Chem.*, **75**, 2517 (2003).
12 R. Q. Long and R. T. Yang, *J. Am. Chem. Soc.*, **123**, 2058 (2001).
13 A. Chambers, C. Park, R. K. Baker, and N. M. Rodriguez, *J. Phys. Chem. B*, **102**, 4253 (1998).
14 N. M. Rodriguez, *J. Mater. Res.*, **8**, 3233 (1996).
15 L. Jiang, L. Gao, and J. Sun, *J. Colloid Interface Sci.*, **260**, 89 (2003).
16 H. E. Ries, *Nature (London)*, **226**, 72 (1970).
17 N. P. Chandia, B. Matushiro, and A. E. Vasquez, *Carbohydr. Polym.*, **46**, 81 (2001).
18 H. Ronghua, D. Yumin, and Y. Jianhong, *Carbohydr. Polym.*, **52**, 19 (2003).
19 W. Zhao, C. Song, and P. E. Pehrsson, *J. Am. Chem. Soc.*, **123**, 5348 (2002).
20 V. Georgakilas, N. Tagmatarchis, D. Pantarotto, A. Bianco, J.-P. Briand, and M. Prato, *Chem. Commun.*, **2002**, 3050.
21 M. J. O'Connell, P. Boul, L. M. Ericson, C. Huffman, Y. Wang, E. Haroz, C. Kuper, J. Tour, K. D. Ausman, and R. E. Smalley, *Chem. Phys. Lett.*, **342**, 265 (2001).
22 G. I. Dovbeshko, O. P. Repnytska, E. D. Obraztsova, and Y. V. Shtogun, *Chem. Phys. Lett.*, **372**, 432 (2003).
23 A. Star, D. W. Steuerman, J. R. Heath, and J. F. Stoddart, *Angew. Chem., Int. Ed.*, **14**, 41 (2002).
24 R. Bandypoadhyaya, E. Native-Roth, O. Regev, and R. Yerushalmi-Rozen, *Nano Lett.*, **2**, 25 (2002).
25 N. Nakashima, S. Okuzono, H. Murakami, T. Nakai, and K. Yoshikawa, *Chem. Lett.*, **32**, 456 (2003).

Environ. Sci. Technol. 2004, 38, 6890–6896

Caged Multiwalled Carbon Nanotubes as the Adsorbents for Affinity-Based Elimination of Ionic Dyes

BUNSHI FUGETSU,*,† SHUYA SATOH,† TOSHIKAZU SHIBA,‡,§,∥ TAEKO MIZUTANI,‡ YONG-BO LIN,† NORIFUMI TERUI,† YOSHINOBU NODASAKA,⊥ KATSUSHI SASA,▽ KIYOKO SHIMIZU,○ TSUKASA AKASAKA,⊥ MASANOBU SHINDOH,⊥ KEN-ICHIRO SHIBATA,⊥ ATSURO YOKOYAMA,⊥ MASANOBU MORI,◆ KAZUHIKO TANAKA,◆ YOSHINORI SATO,△ KAZUYUKI TOHJI,△ SHUNITZ TANAKA,† NORIO NISHI,† AND FUMIO WATARI⊥

Graduate School of Environmental Earth Science, Hokkaido University, Sapporo 060-0810, Japan, Frontier Research Division, FUJIREBIO Inc., 51 Komiya, Hachioji, Tokyo 192-0031, Japan, Regenetiss Company, Ltd., 1-5-17 Okaya, Akabane, Nagano 394-0002, Japan, Department of Oral and Maxillofacial Surgery, Matsumoto Dental University School of Dentistry, Matsumoto, Japan, Graduate School of Dental Medicine, Hokkaido University, Sapporo 060-8586, Japan, Otsuka Electronic Company, Ltd., 1-6 Azuma-cho, Hachioji, Tokyo, Japan, Bioscience Division, Hokudo Company, Ltd., Abuta-cho, Abuta-gun, Hokkaido 049-5613, Japan, National Institute of Advanced Industrial Science and Technology at Seto, 110 Nishiibara-cho, Seto 489-0884, Japan, and Graduate School of Environmental Studies, Tohoku University, Sendai 980-8579, Japan

Multiwalled carbon nanotubes (MWCNTs) were used as the active elements for the first time for affinity-based elimination of ionic dyes. MWCNTs were encapsulated in cross-linked alginate (ALG) microvesicles using Ba^{2+} as the bridging ion. The Ba^{2+}–alginate matrix constitutes a cage which holds the physically trapped MWCNTs. The cage carries negative charges on its surface. The cage restricts the access of anions of large molecular weight, such as humic acids, because of electrostatic repulsion. The cage also restricts the access of colloids of large size, because of size exclusion. Ionic dyes partition into the cage and then are captured by MWCNTs probably on the basis of van der Waals interactions occurring between the hexagonally arrayed carbon atoms in the graphite sheet of MWCNTs and the aromatic backbones of the dyes. As a result of these interactions the target species, namely, the ionic dyes, are eliminated efficiently by the MWCNTs of Ba^{2+}–ALG/MWCNT composite adsorbents. The adsorptive capacities for elimination of acridine orange, ethidium bromide, eosin bluish, and orange G (the model species used for this study) were found as high as 0.44, 0.43, 0.33, and 0.31 μmol, respectively, for 1.0 mg of the caged MWCNTs. Adsorptive experiments with carbon nanofibers and activated carbons as the adsorbents were also performed. The MWCNT-based adsorbents provided the best capability for the affinity-based elimination of these targeted species. Biocompatibility experiments performed in vitro and in vivo provided promising results, suggesting potential applications of the caged MWCNTs in in situ environmental remediation.

Introduction

Dyes have long been recognized to be capable of causing environmental contaminations. First, dyes, especially the azo-type dyes (*1*), are suspected to be carcinogenic and are known to have potent acute and/or chronic effects on exposed organisms, depending on the exposure time and dye concentration. Second, dyes are capable of absorbing/reflecting sunlight; this can have a strong detrimental effect on the growth of bacteria to levels sufficient to biologically degrade impurities (*2, 3*). Moreover, dyes are highly visible to the human eye; this can cause aesthetic contamination even at very low concentrations. Wastewaters from colorant industrials (such as from the textile, pulp, paper, and carpet manufacturing industries) contain dyes which should be eliminated to avoid environmental contaminations. A number of promising techniques have been established for elimination of dyes from contaminated waters. Physical adsorption appears to offer the best advantages (*4–7*), although the chemical degradation (*8–10*) and the biodegradation approaches (*11–13*) also find applications.

Here, we report experimental data on the first use of carbon nanotubes as the active elements for affinity-based elimination of dyes. Carbon nanotubes (CNTs) are the tubular derivatives of fullerenes first discovered by Iijima in 1991 (*14*). CNTs can be classified into multiwalled carbon nanotubes (MWCNTs) (*14*) and single-walled carbon nanotubes (SWCNTs) (*15*), according to the graphene layers in the wall of the nanotubes. Because of their unusual morphology and unique electronic, mechanical, and chemical properties, CNTs have been the subject of many theoretical and experimental studies since their discovery. With the great progress in synthesizing/purifying CNTs, attention has been recently directed to their fields of practical applications. So far, potential application of CNTs to environmental protection/remediation has been very little explored. An environmental analytical chemical study of Cai and co-workers demonstrated that cartridges filled with MWCNTs are capable of extracting bisphenol A, 4-*n*-nonylphenol, 4-*tert*-octylphenol (*16*), and several phthalate esters (*17*) from contaminated waters. Cartridges or columns packed with CNTs may provide high elimination capabilities; they are, however, impractical for large-scale water treatment. This is because of the high back-pressure that must be overcome to drive water through the packed cartridges and/or columns. Another adverse factor currently restricting the application of CNTs to environmental

* Corresponding author phone and fax: +81-11-706 2272; e-mail: hu@ees.hokudai.ac.jp.
† Graduate School of Environmental Earth Science, Hokkaido University.
‡ FUJIREBIO Inc.
§ Regenetiss Co., Ltd.
∥ Matsumoto Dental University School of Dentistry.
⊥ Graduate School of Dental Medicine, Hokkaido University.
▽ Otsuka Electronic Co., Ltd.
○ Hokudo Co., Ltd.
◆ National Institute of Advanced Industrial Science and Technology at Seto.
△ Tohoku University.

10.1021/es049554i CCC: $27.50
Published on Web 10/27/2004

protection/remediation is their high costs, which are about 1000 times higher than those of the traditional activated carbons.

These difficulties encountered in environmental applications with CNTs as the active elements were overcome by formation of "caged CNTs". As defined in this laboratory, the caged CNTs are cross-linked alginate vesicles containing physically trapped CNTs. The cross-linked alginate constitutes a polymer "cage", holding physically trapped, highly dispersed CNTs. The polymer cage allows bidirectional diffusion of chemicals of small molecular weight but restricts the freedom of kinetic distribution of molecules and/or colloids of large size. Ionic dyes partition into the vesicles and then are captured by CNTs on the basis of affinity-based adsorption. Humic acids and colloidal particles, on the other hand, are unable to diffuse across the cage. This provides a desirable approach to protect the active elements from being damaged by adsorbing chemicals and/or colloids of large size. The caging (encapsulating) technique is also a practical approach to overcome the high cost and/or high-pressure difficulties encountered in the use of CNTs for environmental remediation.

Materials and Methods

Dispersion of MWCNTs Using Alginate. Sodium alginate (the viscosity and pH at 28 °C were 376 cP and 7.10, respectively, for a 10.0 mg/mL aqueous solution) was obtained from Wako Chemical Industries (Osaka, Japan). Sodium alginate (Na^+−ALG) was dissolved in deionized water to prepare the aqueous Na^+−ALG solution at a concentration of 10.0 mg/mL. MWCNTs (CVD products, outer diameter 15 ± 5 nm, length 1−5 μm, purity >90%, as stated by the manufacturer) were purchased from Nanolab (Massachusetts) and were used as received. MWCNTs were introduced to an aqueous Na^+−ALG (10.0 mg/mL) solution and were then well-mixed by a combination of high-shear mixing and sufficient ultrasonication. The uniformity of the aqueous Na^+−ALG/MWCNT colloids was measured by calculating the linearity of the calibration curve for MWCNTs in the Na^+−ALG/MWCNT colloidal solutions using UV−vis at 254 nm as the detection method. ζ potentials of the aqueous Na^+−ALG/MWCNT colloids were measured using an electrophoretic light scattering spectrophotometer (ELS-8000, Otsuka Electronics, Osaka, Japan). FT-IR spectra of Na^+−ALG in the aqueous Na^+−ALG/MWCNT colloids were measured using an FT/IR-460 (Jasco, Tokyo, Japan).

Preparation of Cross-Linked Alginate Microvesicles. An IER-20 encapsulation system (Inotech, Dottikon, Switzerland) was used for vesicle preparation. The aqueous Na^+−ALG/MWCNTs colloids (precursor solution) were forced into the pulsation chamber using a syringe pump. These aqueous colloids were then passed through a precisely drilled sapphire nozzle (nozzle size 200 μm) and were separated into droplets of equal size on exiting the nozzle. These droplets passed through the electrostatic field between the nozzle and an O-ring electrode and acquired electrostatic charges on their surfaces. Electrostatic repulsion forces dispersed the droplets as they fell into the hardening (coagulation) solution, which was an aqueous solution containing 100 mM barium chloride (see the schematic diagram in Figure 1). The resultant vesicles were rinsed thoroughly with deionized water using a 100 μm mesh sieve. Reference vesicles (without containing MWCNTs), vesicles containing activated carbons, and vesicles containing CNFs were also prepared under identical encapsulation conditions. The activated carbons (activated charcoal, powder) were obtained from Wako Chemical Industries, while CNFs (diameter 50−250 nm, length 2−15 μm, purity >90%) were synthesized in the laboratory on the basis of the chemical vapor deposition method (*18*). The Ba^{2+}−ALG vesicles are both mechanically and chemically stable, and

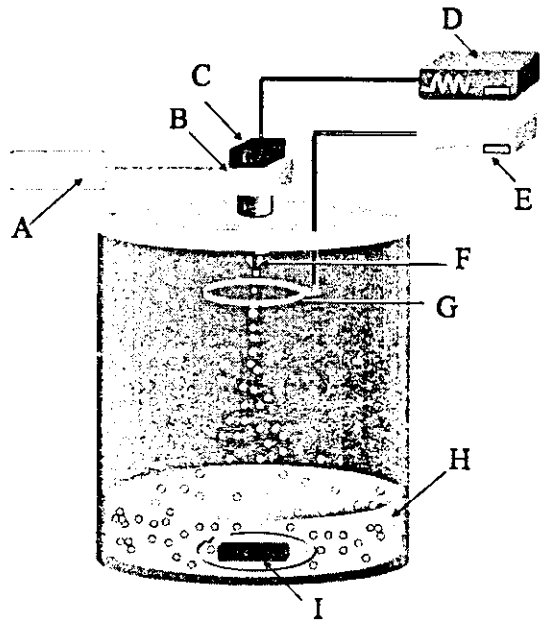

FIGURE 1. Schematic diagram of the encapsulation system: (A) syringe pump; (B) pulsation chamber; (C) vibration system; (D) frequency generator; (E) electrostatic charge generator; (F) nozzle; (G) O-ring electrode; (H) coagulation solution; (I) magnetic stirrer.

are much heavier than water; hence, it is easy to isolate the vesicles from the treated water.

Biocompatibility Studies. Balb c/3T3 cells were used to perform the in vitro experiments. The cells were seeded to 48-multiwell plates at 6000 cells/well (300 μL/well) and cultured in Dulbecco's modified Eagle's minimal essential medium (DMEM) containing 10% fetal bovine serum (FBS) for 3 days at 37 °C. The media containing the alginate vesicles were prepared by suspending 100, 50, and 10 mg of vesicles in 1.0 mL of DMEM containing 10% FBS to give solutions containing 100, 50, and 10 mg/mL alginate vesicles, respectively. The medium of the 48-multiwell plates was replaced with 300 μL of the media containing the alginate vesicles, and the cells were further incubated at 37 °C. After 48 h of incubation, the cell proliferation was evaluated by 3-(4,5-dimethylthiazol-2-yl)-5-(3-carboxymethoxyphenyl)-2-(4-sulfophenyl)-2*H*-tetrazolium (MTS) assay. For MTS assay, the media were replaced with 100 μL of Eagle's minimal essential medium (without Phenol Red), and 25 μL of a mixture of MTS (Promega) and phenazine methosulfate solution (2.0 mg/mL MTS, 0.92 mg/mL phenazine methosulfate) was added to each well. After incubation for 1 h at 37 °C, the absorbance at 490 nm of each well was measured. The cell number was quantified by means of the bioreduction activity of viable cells.

Twelve 10-week-old Crj:CD(SD) IGS male rats (purchased from Charles River Japan, Inc.) were used to perform the in vivo experiments. These rats were quarantined and acclimatized for 6 days. Three were used without any administration, while the others were dosed orally using a stomach tube for 1 week. The dose volumes were 5.0 mL/kg of body mass. Gross observations and body masses were recorded daily. During the term of observation, the animals were starved for 16 h and anesthetized, and then blood and serum samples were collected. Necropsy was also performed for observing changes in the glandular stomach.

Adsorption Studies. A given volume of the model-contaminated water containing a known quantity of dye was mixed with a known volume of the vesicles using a 100 mL conical-bottomed test tube. The concentration of dye in the aqueous phase was measured using a UV spectrophotometer (Jasco UV-550). Acridine orange and ethidium bromide

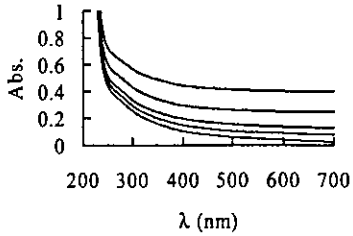

FIGURE 2. UV–vis absorption spectrum of the dispersing solution (which was prepared by dissolving sodium alginate in deionized water at a concentration of 10.0 mg/mL, the bottom trace) and that of the dispersed MWCNTs at concentrations of 100, 50, 25, and 10 ppm (from top to bottom, respectively).

(cationic type) and eosin bluish and orange G (anionic type) were used as the model species to represent the water-soluble, ionic dyes. The adsorptive experiments were performed using Ba^{2+}–ALG composite vesicles (i.e., the control vesicles), Ba^{2+}–ALG vesicles containing MWCNTs (caged MWCNTs), vesicles containing CNFs (caged CNFs), and vesicles containing activated carbons (caged ACTC) as the adsorbents. Humic acids (HAs; obtained from Wako Chemical Industries) were used as the model species to represent water-soluble, naturally occurring compounds of high molecular weights.

Encapsulation of CNTs in Ba^{2+}–ALG vesicles is a desirable approach to restrain adsorbents of small size; this, however, may create mass-transfer problems. To figure out this point, the adsorptive experiments were also performed using the as-purchased MWCNTs (also CNFs and activated carbons) as the adsorbents. A high-pressured filtration process (the aqueous solution containing dye mixed with MWCNTs, CNFs, or activated carbons was filtered through two stacked polycarbonate filters of 100 nm pore size) was necessary to remove the adsorbents.

Results and Discussion

Aqueous Alginate/MWCNT Colloids. Normally, CNTs (including both SWCNTs and MWCNTs) are seen as powders of visible size because of the strong van der Waals attractions occurring among the individuals. To encapsulate CNTs in vesicles, it was necessary to disperse CNTs with high uniformity in the encapsulating solutions. Approaches to dispersion of CNTs in organic solutions have been developed, mainly based on chemical attachment of appropriate blocks to the carboxylic groups (which are produced by oxidation of CNTs using strong acids) (*19*, *20*). The so-called side-wall organic functionalization technique (*21*, *22*) also finds application. On the other hand, wrapping of water-soluble polymers around CNTs is a simpler yet powerful technique for dispersing CNTs in aqueous solutions. Polymers used in previous studies for CNT dispersion are poly(vinylpyrrolidone) (PVP), poly(styrenesulfonate) (PSS) (*23*), deoxyribonucleic acid (DNA) (*24–26*), starch (*27*), and Arabic gum (*28*). In this study, we use alginate for dispersing the as-purchased powders of entangled CNTs in aqueous solutions. The uniformity of MWCNTs in the aqueous alginate solution was calculated by measuring the linearity of the calibration curve for MWCNTs in the aqueous Na^+–ALG/MWCNT colloidal solutions at 254 nm. The linearity, r^2, was found to be better than 0.9981, indicating MWCNTs were being dispersed in the aqueous Na^+–ALG colloidal solutions with high uniformity. Samples used for deriving the calibration curve were the aqueous Na^+–ALG solutions containing 0, 10, 25, 50, and 100 ppm MWCNTs, with the concentration of Na^+–ALG in each sample being fixed at 10.0 mg/mL. Figure 2 shows UV–vis absorption spectra of the samples; a characteristic absorption derived from the dispersed MWCNTs is seen around 254 nm. The stability of the aqueous Na^+–ALG/MWCNT colloids was measured by calculating the concentration of the MWCNTs versus the sediment time, similar to the method reported by Jiang and co-workers (*29*). Changes in the MWCNT concentrations were found to be smaller than 1.3% over 7 days at room temperature.

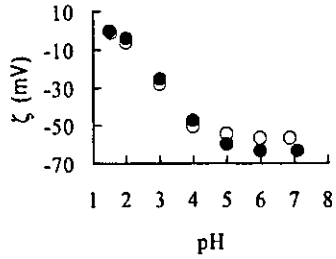

FIGURE 3. ζ potential of the Na^+–ALG/MWCNT colloids (●; MWCNTs, 100 ppm; Na^+–ALG, 10.0 mg/mL) and ζ potential of the dispersing solution (○; Na^+–ALG alone, 10.0 mg/mL) as a function of pH.

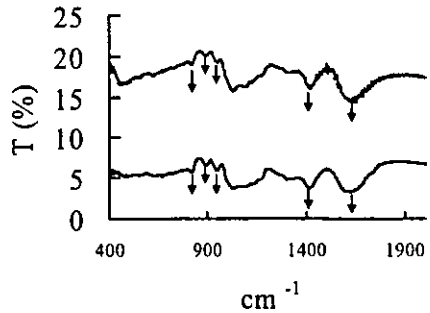

FIGURE 4. FT-IR spectra of Na^+–ALG (upper trace) and Na^+–ALG/MWCNT colloids (lower trace) in the solid state using the potassium bromide (KBr) pellet method.

The ζ potential was measured by calculating the colloid velocities on the basis of the Helmholtz–Smoluchowski equation ($\zeta = 4\pi\mu\eta/D$, where μ, η, and D are the electrophoretic mobility, viscosity, and dielectric constant of the liquid in the boundary layer, respectively) (*30*). The ζ value for the Na^+–ALG/MWCNT colloids was found to be as high as −63.50 mV. This again indicates the high stability of the Na^+–ALG/MWCNT colloids. Figure 3 shows the ζ versus pH plots for the Na^+–ALG/MWCNT colloids and that for the aqueous solution containing Na^+–ALG alone. At higher pH values (5.01, 6.02, 7.10), the alginate/MWCNT colloids showed slightly higher absolute ζ potentials than the sample containing sodium alginate alone, while, at the lower pH values, the ζ potentials for both samples were virtually identical. A decrease in the absolute value of ζ is seen for both samples as the pH decreases (the pH values of the samples were adjusted using 1.0 M HCl). MWCNTs precipitated as the pH reached 2.01 and 1.51. The high ζ potential value and thereby the high stability of the alginate/MWCNT colloids are a result of formation of alginate/MWCNT complexes in the colloidal solution. FT-IR spectral measurement (Figure 4) gives chemical evidence to support this conclusion. Frequencies of the carboxylic group of alginate for the alginate/MWCNT sample shifted from 1628.6 and 1417.4 cm^{-1} to 1618.9 and 1413.5 cm^{-1}, indicating alginate interacting with MWCNTs. On the other hand, the frequency of the α 1–4 linkage for the alginate/MWCNT sample decreased from 949.8 to 945.8 cm^{-1}, suggesting the interaction of alginate with MWCNTs is governed by the hydrophobic sugar backbones of alginate. The frequency of β-mannuronic residues (M) at 892.9 cm^{-1} and that of α-guluronic residues (G) at 815.7 cm^{-1} were observed, suggesting the alginate used for this study is built up in the M–G–M arrangement (*31*, *32*).

Biocompatibility of the Caged MWCNTs Adsorbents of high biocompatibility are highly desirable for in situ environmental remediation. In the in vitro experiments with Balb

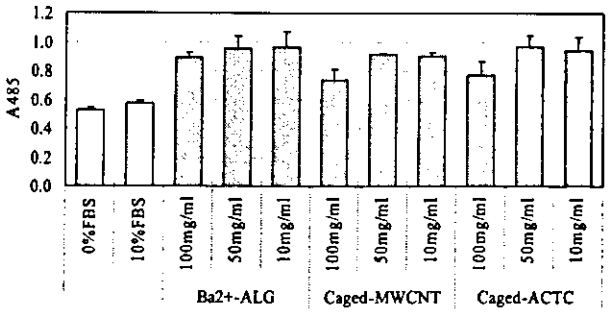

FIGURE 5. Effects of Ba^{2+}–ALG vesicles, caged MWCNTs, and caged ACTC on cell proliferation.

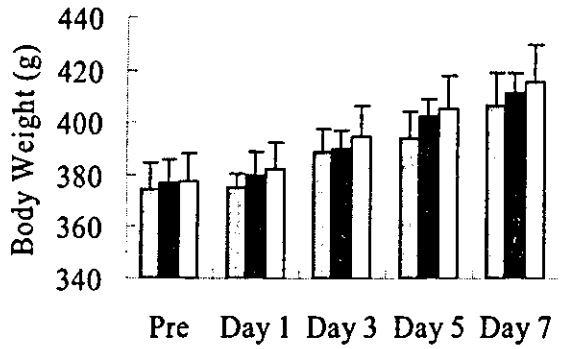

FIGURE 6. Body mass changes as a function of the number of dosed days. The rats were treated with the Ba^{2+}–alginate control vesicles (left-hand column), caged MWCNTs (central column), and caged ACTC (right-hand column).

c/3T3 cells as the typical cells, cells cultured with the caged MWCNTs showed higher cell density than cells cultured without the vesicles (Figure 5). Similar results were also observed for cells cultured with the control vesicles (Ba^{2+}–alginate vesicles) and vesicles containing activated carbons (caged ACTC). The vesicle provided some beneficial effects on cell attachment/growth, and as a result, higher cell densities were provided. The media containing caged MWCNTs and caged ACTC at 100 mg/mL gave lower cell densities than the media containing the control vesicles at the same concentration. The caged MWCNTs and the caged ACTC may adsorb the essential factors, such as the trace amount of growth factors, for cell growth. On the other hand, in the in vivo experimental study with rats as the typical animals, the caged MWCNTs and the caged ACTC showed some enhancement effects on body mass gain (Figure 6). Hematological data and biochemical data for the vesicle-dosed rats were found to be identical to those for the untreated rats (the verification values were $< \pm 8.9\%$, $n = 3$). A change of the deep plica of the glandular stomach was not observed for the vesicle-dosed rats. Both in vitro and in vivo experiments demonstrated that the caged MWCNTs (also the caged ACTC and the Ba^{2+}–alginate vesicles) are highly biocompatible with the cells/animals studied in this study.

Adsorption Studies. Four precursor solutions, (i) an aqueous solution containing sodium alginate alone at 10.0 mg/mL, (ii) MWCNTs, (iii) CNFs, and (iv) ACTC, each at 0.1 mg/mL, being highly dispersed in 10.0 mg/mL Na^+–ALG solution, were prepared and used for preparing the reference vesicles (Ba^{2+}–ALG), caged MWCNTs, caged CNFs, and caged ACTC, respectively. A typical microscopic observation of the vesicles containing MWCNTs, i.e., the caged MWCNTs, is shown in Figure 7. Vesicles having a diameter in the range of 400–600 μm were observed. The nozzle diameter strongly influenced the vesicle size. Generally, vesicles are produced with an average diameter 2 times larger than the nozzle diameter. However, the average vesicle diameter can be adjusted by about ±20% by varying the jet velocity and the vibration frequency. Kilogram quantities of the vesicles can be produced within a few hours using this encapsulation system.

A 15 mL sample of model-contaminated water (prepared by dissolving acridine orange (AO) in deionized water at a concentration of 10.0 μM) was mixed with 3.0 mL of the vesicles. About 30 min after the mixing, approximately 3 mL of the bulk-phase solution was collected and measured using a UV–vis spectrometer. Figure 8 shows the results. The absorbance of the model-contaminated water before the treatment, i.e., the 10.0 μM AO aqueous solution, at 492 nm, was as high as 0.38. This value, however, dropped to 0.037 and 0.042 after this solution was mixed with the vesicles containing MWCNTs and the vesicles containing CNFs, respectively. Vesicles containing activated carbons also showed the ability to lower the absorbance (which dropped to 0.071). This change, however, was smaller than that observed for the vesicles containing MWCNTs (also the vesicles containing highly dispersed CNFs). The control vesicles showed very little capability in trapping AO, suggesting the uptake of the targeted species is governed by the carbon particles. The capability in trapping ethidium bromide ((ET)Br) from the contaminated water was also found in the order caged MWCNTs > caged CNFs > caged ACTC ≫ control vesicles.

Figure 9 shows the experimental data on elimination of eosin bluish (EOB) obtained by mixing 15 mL of the model-contaminated water (prepared by dissolving EOB in deionized water at a concentration of 10.0 μM) with 3.0 mL of the vesicles. The caged MWCNTs showed the highest adsorptive capabilities, followed by the caged ACTC and then the caged CNFs, for elimination of EOB. The control vesicles (Ba^{2+}–ALG) showed no capability for adsorbing EOB. Similar results were also observed for elimination of orange G (OG).

The Ba^{2+}–ALG cage showed some detrimental (resistant) effects on mass transfer for elimination of anionic dyes (EOB and OG). This was observed by comparison of the rates of uptake of EOB using the caged MWCNTs and the as-purchased MWCNTs (MWCNT powder alone) as the active element. As can be seen in Figure 10A, the uptake of the targeted species was accomplished within 10 min when the MWCNT powders alone were used as the adsorbent. It, however, took 23 min to achieve the goal when the caged MWCNTs were used.

The resistant effects on mass transfer were extremely large for anions of large molecular weight. This was observed experimentally using HAs as the targeted species. As can be seen in Figure 10B, HAs showed high affinity toward MWCNTs in the powder forms but no affinity toward MWCNTs in the caged form. In other words, HAs were unable to diffuse across the Ba^{2+}–alginate cage. HAs exclusion can be attributed to the electrostatic repulsion and/or the size exclusion effect of the Ba^{2+}–ALG matrix. The selective permeation properties of the cage provide a desirable approach to protection of the active elements from being damaged by adsorbing chemicals of large molecular weights.

Table 1 summarizes the ultimate capacity for elimination of AO, (ET)Br, EOB, and OG for 1.0 mg of MWCNTs used in the caged and/or powder forms. Experimental data on the ultimate adsorptive capacity for the activated carbons and CNFs are also given in Table 1 for comparison. MWCNTs showed the highest capabilities for elimination of both the cationic and anionic types of the model species; this was irrespective of whether the powder form or the caged form was used as the adsorbent. CNFs gave higher capabilities than activated carbons for elimination of the cationic type of dyes (namely, AO and (ET)Br). On the other hand, however, activated carbons showed higher capabilities than CNFs for elimination of the anionic type of dyes (i.e., EOB and OG).

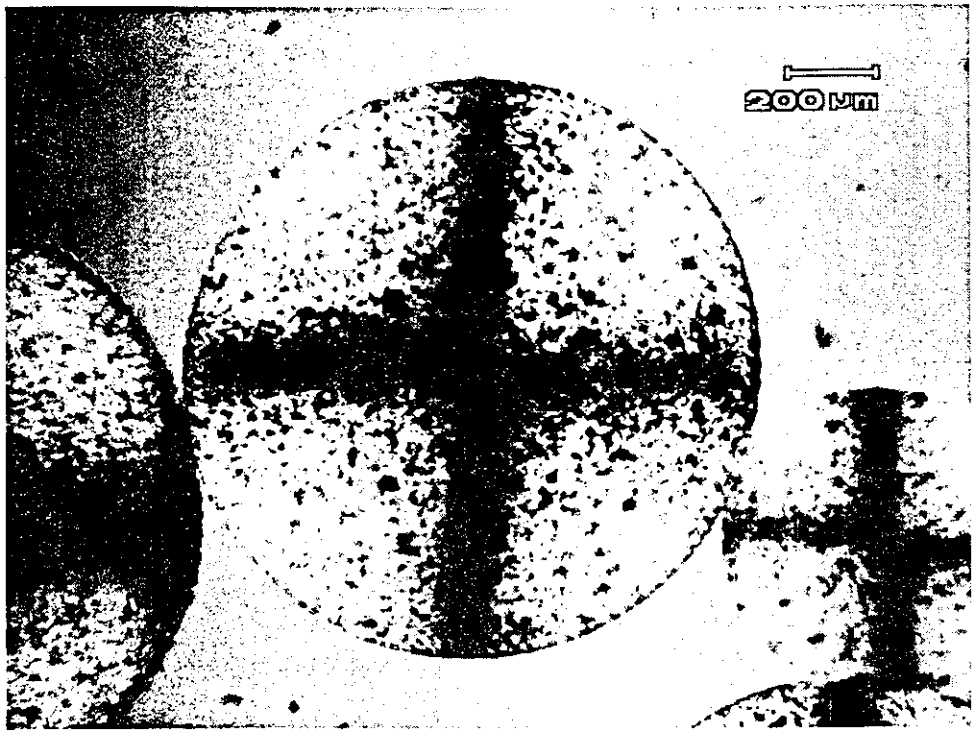

FIGURE 7. Microscopic observation of the Ba^{2+}–alginate-coated vesicles containing highly dispersed MWCNTs. The vesicles were produced using an aqueous colloidal solution containing 0.10 mg/mL (namely, 100 ppm) MWCNTs and 10.0 mg/mL Na^{+}–ALG as the precursor solution with an aqueous solution containing 100 mM $BaCl_2$ as the coagulation solution.

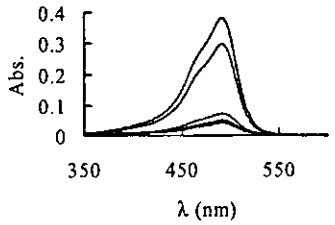

FIGURE 8. UV–vis absorption spectrum of an aqueous solution containing 10.0 μM AO and that of 15 mL of this 10.0 μM AO solution mixed with Ba^{2+}–alginate vesicles (reference vesicles), caged ACTC, caged CNFs, and caged MWCNTs (from top to bottom, respectively) 30 min after the solution/vesicle mixing.

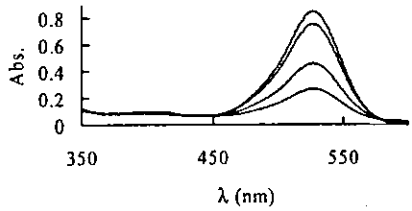

FIGURE 9. UV–vis absorption spectrum of an aqueous solution containing 10.0 μM EOB and that of 15 mL of this 10.0 μM EOB solution mixed with 3.0 mL of caged CNFs, caged ACTC, and caged MWCNTs (from top to bottom, respectively) 30 min after the solution/vesicle mixing. Note that the solution mixed with Ba^{2+}–alginate vesicles (reference vesicles) showed an absorption spectrum identical to that of the untreated solution.

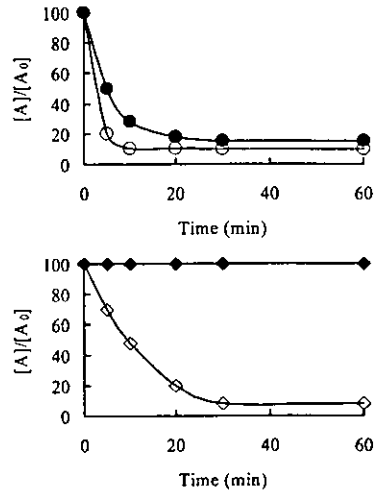

FIGURE 10. (A) Effects of the Ba^{2+}-cross-linked alginate cage on the rate of uptake of EOB by MWCNTs: (●) MWCNTs encapsulated in the cage; (○) MWCNTs alone. [A_0] = the initial concentration of EOB. [A] = the concentration of EOB in the aqueous solution found after the solution was mixed with the adsorbents. (B) Effects of the Ba^{2+}-cross-linked alginate cage on the rate of uptake of HAs by MWCNTs: (◆) MWCNTs encapsulated in the cage; (◇) MWCNTs alone. [A_0] = the initial concentration of HAs. [A] = the concentration of HAs in the aqueous solution found after the solution was mixed with the adsorbents.

MWCNTs offer the best capabilities for adsorbing dyes. This can be attributed to the fact that the hexagonally arrayed carbon atoms in the graphite sheets of MWCNTs are the active sites for trapping the targets. CNFs are built up also by hexagonally arrayed carbon atoms, but the 002 planes pile up along the direction of the fiber axis. These graphite platelets stack in a unique conformation in which only the edge sites are exposed (*33*). CNFs are typically highly defective and therefore should have a considerably large number of carboxylic groups on the exposed edges of the purified CNFs. The carboxylic groups are the beneficial sites for elimination of cationic dyes, and as a result, higher capabilities for elimination of AO and (ET)Br are obtained. These negatively charged groups, however, can have resistant effects on mass transfer for anionic dyes. The very low capability to eliminate EOB and OG by the CNF-based adsorbents gives the experimental evidence to support this conclusion.

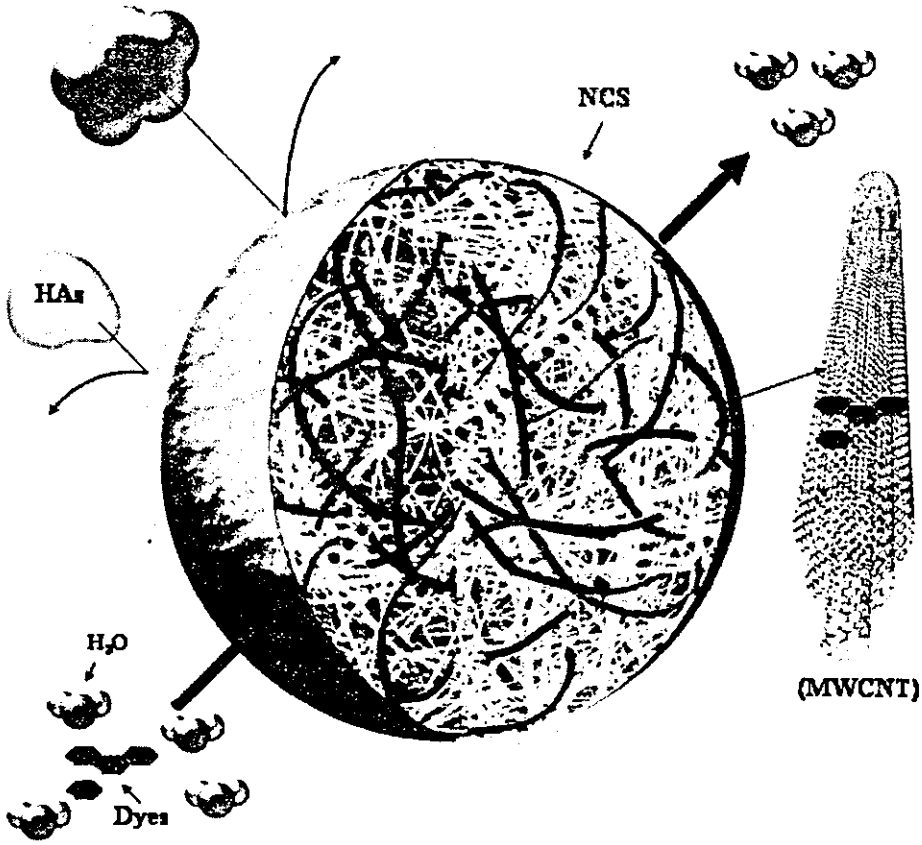

FIGURE 11. Schematic representation of the advantageous performances of the caged MWCNTs. The Ba^{2+}−alginate cross-linked matrix constitutes a cage which holds the physically trapped MWCNTs. The cage carries negative charges (NCS) on its surface. The cage restricts the access of anions of large molecular weights, such as HAs, because of electrostatic repulsion. The cage also restricts the access of CLS because of size exclusion. Dyes partition into the cage and are captured by MWCNTs probably on the basis of van der Waals interactions occurring between the hexagonally arrayed carbon atoms in the graphite sheet of MWCNTs and the aromatic backbones of the dyes. As a result of these interactions the target species, namely, the ionic dyes, are eliminated efficiently by the MWCNTs of the MWCNT/Ba^{2+}−ALG composite adsorbents.

TABLE 1. Adsorptive Capacity (μmol/mg) of MWCNTs, CNFs, and ACTC for Elimination of the Ionic Dye[a]

	MWCNT-P	C-MWCNT	CNF-P	C-CNF	ACTC-P	C-ACTC
AO	0.39	0.44	0.38	0.43	0.36	0.39
(ET)Br	0.37	0.43	0.36	0.42	0.35	0.37
EOB	0.37	0.33	0.09	0.06	0.25	0.19
OG	0.35	0.31	0.07	0.04	0.22	0.15

[a] Average values of three measurements (RSD < 1.8%). MWCNT-P = MWCNTs in the powder form (MWCNTs alone), and C-MWCNT = MWCNTs encapsulated in the cross-linked Ba^{2+}−alginate vesicle. CNF-P, ACTC-P, C-CNF, and C-ACTC have the same meanings as for MWCNTs. AO = acridine orange, (ET)Br = ethidium bromide, EOB = eosin bluish, and OG = orange G.

A model, as shown in Figure 11, is proposed to summarize the advantageous performances of the caged MWCNTs for elimination of the ionic dyes. The affinity elements, namely, MWCNTs, are encapsulated in Ba^{2+}−alginate vesicles of submillimeter size. This provides a desirable approach to restrain adsorbents of nanosize. The Ba^{2+}-cross-linked alginate matrix constitutes a cage. This cage restricts the access of anions of large molecular weight (also colloids of large size, CLS) while it allows the bidirectional distribution of chemicals of small molecular weights. HAs exclusion is probably due to the negatively charged surface (NCS) of the cage, although size exclusion may also be a possible explanation. Dyes were eliminated by MWCNTs probably on the basis of van der Waals attractions occurring between the aromatic backbones of dyes and the hexagonally arrayed carbon atoms in the graphite sheets of the MWCNTs. In addition, the caged MWCNTs could be reused by regenerating the vesicles with aqueous methanol or acetonitrile solutions. The caged MWCNTs may also be applicable for in situ elimination of dyes and/or other types of aromatic pollutants from the contaminated animal bodies. Experimental studies on the possibility of using the caged MWCNTs for in situ environmental remediation are under evaluation.

Acknowledgments

The very helpful comments provided by the reviews of this manuscript are gratefully acknowledged. This study was partly supported by a Grant-in-Aid for Research on Nanomedicine (No. H14-nano-021) from the Ministry of Health, Labor and Welfare of Japan.

Literature Cited

(1) Brown, M. A.; De Vito, S. C. Predicating azo dye toxicity. *Crit. Rev. Environ. Sci. Technol.* **1993**, *23*, 249−324.
(2) Slokar, Y. M.; Le Marechal, M. Methods of decolouration of textile wastewaters. *Dyes Pigm.* **1998**, *37*, 335−356.
(3) Strickland, A. F.; Perkins, W. S. Decolouration of continuous dyeing wastewater by ozonation. *Text. Chem. Color.* **1995**, *27*, 11−19.
(4) Pandit, P.; Basu, S. Removal of ionic dyes from water by solvent extraction using reversed micelles. *Environ. Sci. Technol.* **2004**, *38*, 2435−2442.
(5) Gupta, V. K.; Srivastava, S. K.; Mohan, D. Equilibrium uptake, sorption dynamics, process optimization, and column operations for the removal and recovery of malachite green from

wastewater using activated carbon and activated slag. *Ind. Eng. Chem. Res.* **1997**, *36*, 2207−2218.
(6) Garg V. K.; Amita M.; Kumar R.; Gupta R. Basic dye (methylene blue) removal from simulated wastewater by adsorption using Indian Rosewood sawdust: a timber industry waste. *Dyes Pigm.* **2004**, *63*, 243−250.
(7) Poots, V. J. P.; McKay, G.; Healy, J. J. The removal of acid dye from effluent using natural adsorbents-I peat. *Water Res.* **1976**, *10*, 1061−1066.
(8) Karkmaz, M.; Puzenat, E.; Guillard, C.; Herrmann, J. M. Photocatalytic degradation of the alimentary azo dye amaranth mineralization of the azo group to nitrogen. *Appl. Catal., B: Environ.* **2004**, *51*, 183−194.
(9) Zheng S.; Huang Q.; Zhou J.; Wang B. A study on dye photoremoval in TiO_2 suspension solution. *J. Photochem. Photobiol., A: Chem.* **1997**, *108*, 235−238.
(10) Ruppert G.; Bauer, R.; Heisler, G. UV-O_3, UV-H_2O_2, UV-TiO_2 and the photo-fenton reaction-comparison of advanced oxidation processes for wastewater treatment. *Chemosphere* **1994**, *28*, 1447−1454.
(11) More, A. T.; Vira, A.; Fogel, S. Biodegradation of *trans*-1,2-dichloroethylene by methane-utilizing bacteria in an aquifer simulator. *Environ. Sci. Technol.* **1989**, *23*, 403−406.
(12) Patil, S. S.; Shinde, V. M. Biodegradation studies of aniline and nitrobenzene in aniline plant waste water by gas chromatography. *Environ. Sci. Technol.* **1988**, *22*, 1160−1165.
(13) An H.; Qian Y.; Gu X.; Tang W. Z. Biological treatment of dye wastewaters using an anaerobic-oxic system. *Chemosphere* **1996**, *33*, 2533−2542.
(14) Iijima, S. Helical microtubules of graphitic carbon. *Nature (London)* **1991**, *354*, 56−58.
(15) Iijima, S.; Ichihashi, T. Single-shell carbon nanotubes of 1-nm diameter. *Nature (London)* **1993**, *363*, 603−605.
(16) Cai, Y.; Jiang, G.; Liu, J.; Zhou, Q. Multi-walled carbon nanotubes as a solid-phase extraction adsorbent for the determination of bisphenol A, 4-*n*-nonylphenol, and 4-*tert*-octyphenol. *Anal. Chem.* **2003**, *75*, 2517−2521.
(17) Cai, Y.; Jiang, G.; Liu, J.; Zhou, Q. Multi-walled carbon nanotubes packed cartridge for the solid-phase extraction of several phthalate esters from water samples and their determination by high-performance liquid chromatography. *Anal. Chim. Acta* **2003**, *494*, 149−156.
(18) Rodriguez, N. M. A review of catalytically grown carbon nanofibers. *J. Mater. Res.* **1993**, *8*, 3233−3250.
(19) Chen, J.; Hamon, M. A.; Hu, H.; Chen, Y.; Rao, A. M.; Eklund, P. C.; Haddon, A. Solution properties of single-walled carbon nanotubes. *Science* **1998**, *282*, 95−98.
(20) Zhao, W.; Song, C.; Pehrsson P. E. Water-soluble and optically pH-sensitive single-walled carbon nanotubes from surface modification. *J. Am. Chem. Soc.* **2002**, *124*, 12418−12419.
(21) Chen R. J.; Zhang Y.; Wang D.; Dai H. Noncovalent sidewall functionalization of single-walled carbon nanotubes for protein immobilization. *J. Am. Chem. Soc.* **2001**, *123*, 3838−3839.
(22) Georgakilas, V.; Tagmatarchis, N.; Pantarotto, D.; Bianco, A.; Briand, J.-P.; Prato, M. Amino acid functionalisation of water soluble carbon nanotubes. *Chem. Commun.* **2002**, 3050−3051.
(23) O'Connell, M. J.; Boul, P.; Ericson, L. M.; Huffman, C.; Wang, Y.; Haroz, E.; Kuper, C.; Tour, J.; Ausman, K. D.; Smalley, R. E. Reversible water-solubilization of single-walled carbon nanotubes by polymer wrapping. *Chem. Phy. Lett.* **2001**, *342*, 265−271.
(24) Dovbeshko, G. I.; Repnytska, O. P.; Obraztsova, E. D.; Shtogun, Y. V. DNA interaction with single-walled carbon nanotubes: a SEIRA study. *Chem. Phys. Lett.* **2003**, *372*, 432−437.
(25) Nakashima, N.; Okuzono, S.; Murakami, H.; Nakai, T.; Yoshikawa, K. DNA dissolves single-walled carbon nanotubes in water. *Chem. Lett.* **2003**, *32*, 456−457.
(26) Zheng, M.; Jagota, A.; Strano, M. S.; Santos, A. P.; Barone, P.; Chou, S. G.; Diner, B. A.; Dresselhaus, M. S.; Mclean, R. S.; Onoa, G. B.; Samsonidze, G. G.; Semke, E. D.; Usrey, M.; Walls, D. J. Structure-based carbon nanotubes sorting by sequence-dependent DNA assembly. *Science* **2003**, *302*, 1545−1548.
(27) Star, A.; Steuerman, D. W.; Heath, J. R.; Stoddart J. F. Starched carbon nanotubes. *Angew. Chem., Int. Ed.* **2002**, *14*, 2508−2512.
(28) Bandypoadhyaya, R.; Native-Roth, E.; Regev, O.; Yerushalmi-Rozen, R. Stabilization of individual carbon nanotubes in aqueous solutions. *Nano Lett.* **2002**, *2*, 25−28.
(29) Jiang, L.; Gao, L.; Sun, J. Production of aqueous colloidal dispersion of carbon nanotubes. *J. Colloid Interface Sci.* **2003**, *260*, 89−94.
(30) Ries, H. E. Microelectrophoresis measurements on polymeric flocculants alone and in excess with model colloids. *Nature (London)* **1970**, *226*, 72−73.
(31) Ronghua, H.; Yumin, D.; Jianhong, Y. Preparation and in vitro anticoagulant activities of alginate sulfate and its quaterized derivatives. *Carbohydr. Polym.* **2003**, *52*, 19−24.
(32) Chandia, N. P.; Matushiro, B.; Vasquez, A. E. Alginic acids in Lessonia Trabeculate: charaterization by formic acid hydrolysis and FT-IR spectroscopy. *Carbohydr. Polym.* **2001**, *46*, 81−87.
(33) Chambers, A.; Park, C.; Baker, R. K.; Rodriguez, N. M. Hydrogen storage in graphite nanofibers. *J. Phys. Chem. B* **1998**, *102*, 4253−4256.

Received for review March 22, 2004. Revised manuscript received September 14, 2004. Accepted September 14, 2004.

ES049554I